Rapid Estimation of Cylinder Erosion Rates in Abrasive Dust-Laden Streams

Daniel E. Rosner, Pushkar Tandon, and Michael J. Labowsky
Dept. of Chemical Engineering, Yale University, High Temperature Chemical Reaction Laboratory, New Haven, CT 06520

Erosion yield data for particular combinations of target and projectile materials (via laboratory experiments carried out with a narrow-size distribution over the important range of impact velocities and incidence angles), together with recently developed rational correlations for inertial impaction of suspended particles on a cylinder in high Reynolds number crossflow are used to provide a tractable framework for predicting the erosion rates of, say, heat exchanger tubes immersed in particle-laden streams of combustion products. "Universal" results are cast in terms of the following accessible parameters: sensitivity of erosion yield to projectile incident velocity and angle, ratio of mean particle size to the threshold size required for impaction on the cylindrical target, spread of the mainstream particle size distribution (here log-normal), and the characteristic "slip" Reynolds number for the critical size abrasive particle in the mainstream. Applications of the results are illustrated, and several generalizations are discussed.

Introduction, Background, Objectives

Importance of erosion in power generation and chemical propulsion applications

One of the most challenging aspects of the design of high-performance equipment for power generation or propulsion is dealing with the inevitable *erosion* of components exposed to the high-speed flow of gas containing suspended abrasive particles. In the case of pulverized coal-fired power stations, the heat exchanger surfaces (normally tubes of circular cross section) must survive exposure to the extraneous mineral matter originally in the coal for over 10^{-1} Mh of nearly continuous operation (Raask, 1985). Moreover, combustion turbines running on the products of coal-fired fluidized bed combustors must be designed to also survive exposure to the inevitable "carryover" of fragmented sorbent particles used as sulfur "getters." In propulsion applications (e.g., helicopter and/or tank turbine engines) erosion is usually the result of injested (entrained) abrasive particles in the air required for combustion, an eventuality that usually dictates the geometry of an acceptable inlet system. Mention should also be made of the so-called *erosion-corrosion interaction*, that is, erosion of normally corrosion-resistant metal alloy "scales," which in hostile chemical environments can bring about extensive damage by corrosion even when the erosion damage itself would have been tolerable.

Prediction of erosion rates in engineering equipment

In the present article we deal with the engineering "prediction" of erosion rates in particle-laden environments, based upon experimental data on erosion rates when small flat samples are deliberately exposed to impacting particles of selected materials, at nearly one size, one velocity, and one angle of incidence in an erosion test rig (see, e.g., Finnie, 1959; Tabakoff et al., 1979a,b, 1980). Exploiting such data, even when available for the particular materials combinations of interest, to anticipate erosion rates in realistic engineering environments is normally a computationally demanding task since it is necessary to track the impingement frequency, velocity, and incidence angles of all the different size particles in the mainstream capable of striking the target locations of interest, invoking the abovementioned *erosion yield data* at each such point to predict the corresponding cumulative local erosion rate. However, by focusing our attention on the canonical (and extensively studied) geometry of a circular-cy-

Correspondence concerning this article should be addressed to D. E. Rosner.
Current address of M. J. Labowsky: Diamond Productions, Inc., Consolidated Diamond Blade Division, 443 Newark Pompton Turnpike, Wayne, NJ 07470.

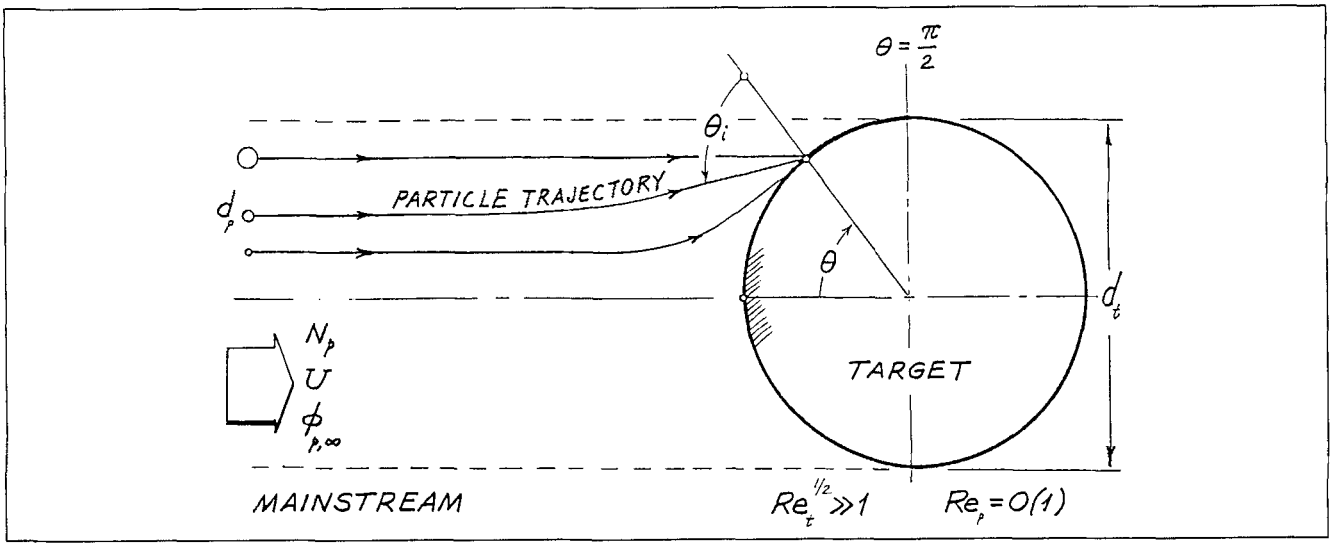

Figure 1. Flow configuration: erosion of a circular cylinder in cross flow of particle-laden gas stream.

lindrical target in cross-flow (Figure 1) and introducing a modest number of defensible approximations (subsections titled "Basic Assumptions and Cases Explicitly Considered," "Erosion Yield Law," and "Examination of Approximations") to summarize the measured erosion yield behavior of the materials of interest, we will show that the tedious portion of such erosion rate predictions can be carried out "once-and-for-all," thereby reducing the engineering problem of predicting target erosion rates to that of multiplying a readily calculated *reference erosion rate* by a set of "universal" dimensionless erosion rate functions calculated and reported here. The reference erosion rate is here chosen to be that which would be associated with the mainstream abrasive particle mass flux if all particles struck the target at the most vulnerable incidence angle (θ_*) with unmodified (mainstream) impact velocity. For convenience, our results will be cast in terms of the following accessible parameters: sensitivity of erosion yield to projectile incident velocity and angle, ratio of mean abrasive particle size to the threshold size required for impaction on the circular-cylinder target in the prevailing flow environment, spread of the mainstream abrasive particle size distribution (here assumed "log-normal"), and the characteristic "slip" Reynolds number for the critical size abrasive particles in the mainstream.

Given these objectives, the present article is structured as follows. In the next section we spell out the principal assumptions underlying our erosion rate analysis, including a presentation/discussion of our choice of *erosion yield law*, the *inertial impaction correlations* used, and the resulting quadrature expressions for the abovementioned erosion rate functions of greatest practical interest. We explicitly consider log-normal populations of abrasive particles suspended in the mainstream and, in part for check purposes, derive the simple limiting forms of our erosion rate results when the particle Stokes number (based on mean particle size) is very large ($\geq 10^2$) and the mainstream particle size distribution is very narrow (i.e., those conditions approached in erosion test rigs, but not appropriate to the engineering applications that concern us here). In the third section we present all of our numerical results (for local, peak and average erosion rates), spanning the dimensionless parameter ranges of greatest practical interest. The utility of these results is illustrated in the fourth section, with the help of a numerical example, which also includes a defense and critical discussion of the assumptions and outlines several straightforward generalizations that may interest the reader. The fifth section concludes the present article with a summary of our principal findings and comments on future work suggested by our present results.

Mathematical Model and Formulation

Basic assumptions and cases explicitly considered

By combining recent results on the impaction of initially suspended particles on the surface of a circular cylinder target in high Reynolds number crossflow with available (if still limited) data on the average erosion yield when individual particles strike solid surfaces (e.g., volume removed per unit volume of arriving particles), it is possible to formulate/calculate the local and total erosion rate for such a target exposed to a flowing suspension of abrasive particles that are "distributed" in size. To capture the essential phenomena in a simple manner without making unrealistic idealizations we make the following basic assumptions (critically examined in the section titled "Examination of Approximations"):

1. Local particle impaction frequencies, velocities, and angle-of-incidence can be calculated with sufficient accuracy from recently available correlations summarizing the results of individual suspended non-Brownian particle trajectories (Fernandez de la Mora and Rosner, 1981) calculated for steady, inviscid flow past an isolated circular cylinder target (Figure 1).

2. The important systematic departures from Stokes drag law (owing to local "slip" Reynolds number that exceeds unity) can be adequately accounted for by using a modified ("effective") Stokes number that corrects for non-Stokesian drag in the computation of the characteristic particle stopping time or distance in the prevailing viscous carrier gas (Israel and Rosner, 1983).

3. Average specific erosion yields (e.g., target volume removed per incident projectile volume) determined by independent erosion experiments at particular velocities and incidence angles can be invoked to predict average erosion yields in engineering applications where abrasive particles arrive simultaneously over a broad *range* of impact velocities and incidence angles.

4. Rebounding particles do not appreciably influence incoming particles, nor cause appreciable downstream erosion upon reimpaction on the same target.

5. Predicted "initial" erosion rate trends (spatial distributions) determined on an initially smooth circular cylinder target can be used to estimate somewhat longer time erosion behavior on inevitably roughened cylinders that depart from circular shape due to localized wear.

6. The mainstream population of suspended abrasive particles is approximately log-normal with respect to particle volume and, while the particle mass loading, ω_p, in the mainstream may not be very small, the *volume fraction*, ϕ_p, corresponding to the total particle number density N_p and mean particle volume $\bar{v}$ (i.e., $\phi_p = N_p \cdot \bar{v}$) *is* negligible.

7. On the scale of the *target* diameter, d_t, the mainstream suspended particles are uniformly distributed in space and are individually negligible in size. However, it is *not* necessary that the average interparticle separation, $N_p^{-1/3}$ be small on the scale of the target cylinder diameter.

Subject to these assumptions, we show that actual local erosion rates (say, in the units: mm recession per year of continuous exposure) at position θ (Figure 1) can be expressed as the product of an easily calculated reference erosion rate $(ER)_{\text{ref}}$ and a universal dimensionless function $E(\theta, \ldots)$ calculated and plotted here over the interesting range of mean suspended particle diameter (expressed as a multiple of critical diameter required for inertial impaction in the prevailing environment). The reference erosion rate is that which would be expected in the prevailing environment if all mainstream particles had a mean size and struck a unit target surface with undiminished speed and at the most vulnerable angle—that is, in the units of linear recession rate:

$$(ER)_{\text{ref}} \equiv \epsilon_p(U, \theta_*) \cdot (\bar{v} N_p U)_\infty \tag{1}$$

where ϵ_p is the *specific erosion yield* (average volume removed per unit volume of projectile particle impacting) evaluated at the particle mainstream velocity U and at incidence angle θ_* (see the subsection on erosion yield law). Thus, the local erosion rate will be $E(\theta, \ldots) \cdot (ER)_{\text{ref}}$, the *peak* local erosion rate (occurring at angular position $\theta_{E_{\max}}$) will be $E_{\max} \cdot (ER)_{\text{ref}}$, and the average erosion rate over the upwind-facing surface will be $\bar{E}(\ldots) \cdot (ER)_{\text{ref}}$.

An attractive feature of this formulation is that the above-mentioned functions E, $E_{\max}$, and $\bar{E}$ can be calculated "once-and-for-all" by straightforward numerical quadratures in terms of an acceptably small number of dimensionless parameters defining the system (application). The availability of these results will be seen to dramatically simplify the task of predicting local and total erosion rates for, say, heat exchanger tubes in the cross-flow of ash-laden combustion products (see the illustrative calculations summarized in the subsection titled "Direct Use to Predict Erosion Behavior").

Erosion yield law

It is not our purpose here to develop further the still incomplete micromechanical theory of erosion yield ϵ_p when particular projectile materials are directed at particular target materials at a known velocity V_p and the angle of incidence θ_i (cf. the outward normal) (see, e.g., Bitter, 1963). Instead, we make use of the main features of such experimental results (Finnie et al., 1967; Tabakoff et al., 1979a,b), namely, the observed functional dependence of specific erosion yield ϵ_p on the particle incident velocity V_p and angle of incidence θ_i, in the projectile particle size range where ϵ_p is independent of d_p (see, e.g., Kotwal and Tabakoff, 1981 and the subsection titled "Generalizations"). A particularly convenient representation of these experimental data for our present purposes is the *separable* form:

$$\epsilon_p = \text{const} \cdot (V_p)^n \cdot f(\theta_i) \tag{2}$$

where the dimensional "constant" is specific to the projectile/target system, the exponent on the particle velocity ($n \equiv \partial \ln \epsilon_p / \partial \ln V_p$, frequently near 2.5) best describes experimental results, especially in the vicinity of the most vulnerable incidence angle θ_*, and the indicated dependence $f(\theta_i)$ on angle of incidence is normalized such that $f(\theta_*) = 1$.

We select the following simple *functional form* for $f(\theta_i)$, characterized by the two parameters θ_* and $f(0) \equiv f_0$ (the value of f at normal incidence):

$$f(\theta_i) = \left\{1 + \delta\left(1 - \frac{\theta_i}{\theta_*}\right)^{3/2}\right\} \cdot \frac{2\left(\dfrac{(\pi/2) - \theta_i}{(\pi/2) - \theta_*}\right)}{1 + \left(\dfrac{(\pi/2) - \theta_i}{(\pi/2) - \theta_*}\right)^2} \qquad \text{for } 0 \le \theta \le \theta_*$$

and

$$f(\theta_i) = \frac{2\left(\dfrac{(\pi/2) - \theta_i}{(\pi/2) - \theta_*}\right)}{1 + \left(\dfrac{(\pi/2) - \theta_i}{(\pi/2) - \theta_*}\right)^2} \qquad \text{for } \pi/2 \ge \theta \ge \theta_*$$

where

$$\delta \equiv \frac{1}{2}\left(1 - \frac{\theta_*}{(\pi/2)}\right)\left[1 + \left(1 - \frac{\theta_*}{(\pi/2)}\right)^{-2}\right] f_0 - 1. \tag{3}$$

The behavior of this simple but realistic function $f(\theta_i)$ is shown in Figures 2 and 3. This simple functional form fits well the erosion rate data obtained from laboratory experiments for a variety of combinations of metal target material and projectile material (Finnie, 1959; Tabakoff et al., 1979a,b, 1980). Note that while we embrace a range of possibilities for $f(0)$ and θ_* (depending upon the relevant failure mechanism: brittle vs. ductile), in all cases we assume that no erosion occurs for projectile particles that strike the surface at

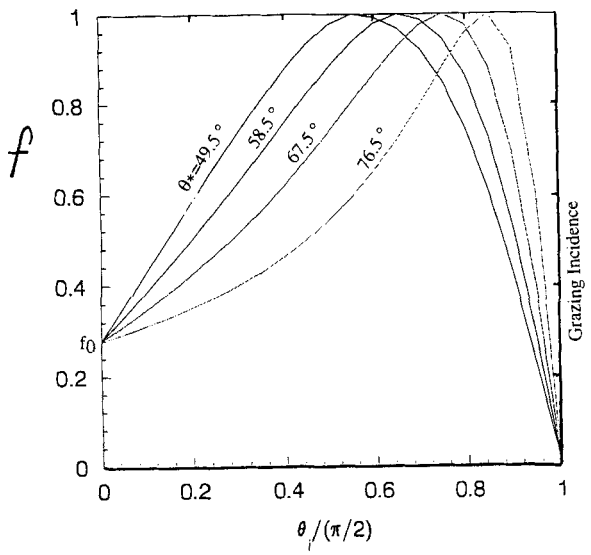

Figure 2. Dependence of erosion yield ϵ_p on projectile angle-of-incidence θ_i for a range of θ_* values.

With $f(\theta_*) = 1$ and constant $f(0)$ (= 0.28); see Eq. 3.

"grazing" incidence ($\theta_i = \pi/2$ radians). Actual best-fit values of the four parameters f_0, θ_*, n, and $\epsilon_{p,\text{ref}}$ extracted from available erosion yield measurements for a variety of metal targets and "erodents" are given by Kho et al. (1994).

To fix ideas we note that for a particular case reexamined in the subsection on "direct" use to predict erosion behavior —namely, Kingston coal ash particles (2.4 g/cm^3) incident upon #304 stainless steel (7.9 g/cm^3)—the experimental data of Tabakoff et al. (1979a,b) in the range 137 m/s $\geq V_p \geq$ 85 m/s indicate $\theta_* \approx 1.15(66°)$, $f(0) \approx 0.28$, $n \approx 2.5$. The absolute peak erosion yield (quoted in mg/g) corresponds to $\epsilon_p \approx 4.9\times10^{-5}$ at $V_p = 120$ m/s and $\theta_i = \theta_* = 1.15$ so that "constant" in Eq. 2 has the approximate numerical value 3.1×10^{-10} (m/s)$^{-2.5}$ for this system. We also immediately find that the reference erosion yield, $\epsilon_p(U, \theta_*)$, evaluated at, say, $U = 10$ ms^{-1} (see the subsection titled "'Direct' Use to Predict Erosion Behavior") is 0.98×10^{-7}. The actual average erosion yield will be less than this figure by a factor closely related to the abovementioned function $\bar{E}$, evaluated below.

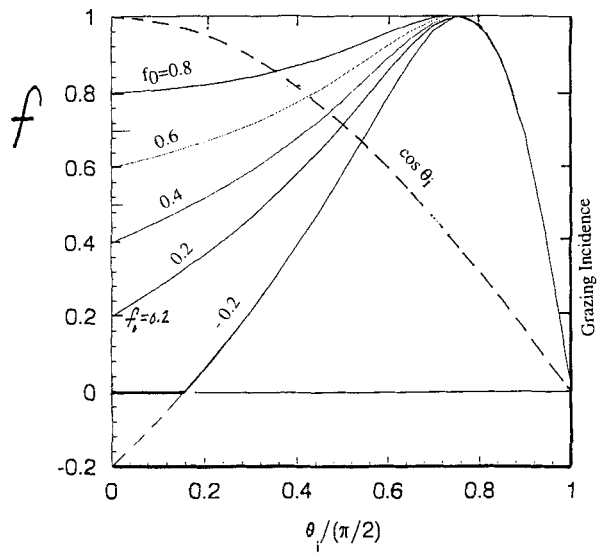

Figure 3. Dependence of erosion yield ϵ_p on projectile angle-of-incidence θ_i for a range of $f(0)$ values.

With $f(\theta_*) = 1$ and constant θ_*; see Eq. 3.

In what follows, results will be shown for the following representative ranges of the abovementioned erosion yield parameters: $55° \leq \theta_* \leq 75°$, $2 \leq n \leq 3$, $0.2 \leq f(0) \leq 0.8$ straddling the abovementioned "typical" values. These graphs, together with a compendium of the four parameters, f_0, θ_*, n, and $\epsilon_{p,\text{ref}}$, summarizing erosion yield data (Kho et al., 1994), should permit rapid engineering estimates of target erosion rates for preliminary design/optimization purposes for most combinations of practical interest. However, as discussed in the subsection titled "'Indirect' Use to Infer Parameters in Erosion Yield Law," some of these results, when combined with actual erosion rate observations on test cylinders in a reasonably well-characterized cross-flow, could be used to extract rational estimates of certain of these erosion yield parameters for use in subsequent design/optimization calculations. Inevitably, some cases will require special treatment (e.g., material combinations such that negligible erosion occurs for a range of near-normal incidence angles, corresponding formally to *negative* values of f_0; see Figure 3). This case, among others, will be briefly taken up in the section on the Examination of Approximations, devoted to the defense of our principal approximations and idealizations.

Local and total erosion rate quadrature expression

Consider first the task of predicting the local erosion rate at some arbitrary angular position θ on the target (measured from the forward stagnation line; cf. Figure 1). We write the local impingement flux of particles of volume $v \pm (dv/2)$ as $\eta_{\text{local}}(v, \theta) \cdot UN_p \cdot C_\infty(v)dv$, which corresponds to a volume flux $v\eta_{\text{local}}(v, \theta)UN_p \cdot C_\infty(v)dv$. According to the *erosion yield law* (see the previous subsection) the corresponding contribution to the local erosion rate will be

$$\epsilon_p(V_p(v, \theta), \theta_i(v, \theta)) \cdot v \cdot \eta_{\text{local}}(v, \theta) \cdot UN_p \cdot C_\infty(v)dv \quad (4)$$

and the total local erosion rate will therefore be given by the integral of this integrand over the entire particle volume range $0 \rightarrow \infty$, keeping in mind that, for *inertial impaction*, the integrand (because of $\eta_{\text{local}}(v, \theta)$), is essentially zero below some threshold volume v_{crit} corresponding to $Stk_{\text{crit,eff}} \approx 1/8$. Thus:

$$ER = \int_0^\infty \epsilon_p(V_p(v, \theta), \theta_i(v, \theta)) \cdot v \cdot \eta_{\text{local}}(v, \theta) \cdot UN_p \cdot C_\infty(v)\, dv. \quad (5)$$

A suitable *reference erosion rate* will clearly be

$$(ER)_{\text{ref}} \equiv \epsilon_p(U, \theta_*) \cdot (\bar{v}N_pU)_\infty \quad (6)$$

where the product $(\bar{v}N_p)_\infty$ will be recognized as the main-

stream *particle volume fraction* $\phi_{p,\infty}$. This implies that it will always be possible to calculate actual erosion rates from the product relation:

$$ER = (ER)_{\text{ref}} \cdot E\{\theta, \ldots\} \tag{7}$$

where, in view of Eqs. 1, 5, and 6, the *dimensionless* local erosion rate function $E\{\theta\}$ is explicitly given by

$$E\{\theta, \ldots\} \equiv \int_0^\infty \left[\frac{\epsilon_p\{V_p\{v, \theta\}, \theta_i\{v, \theta\}\}}{\epsilon_p\{U, \theta_*\}} \right] \cdot \left(\frac{v}{\bar{v}}\right) \cdot \eta_{\text{local}}\{v, \theta\} \cdot C_\infty\{v\}\, dv \tag{8}$$

an important result to which we will frequently return.

If we now introduce the *separable* erosion yield law (Eq. 2), we note that the first term in the integrand can be simplified to the product of two dimensionless functions:

$$\left[\frac{\epsilon_p\{V_p\{v, \theta\}, \theta_i\{v, \theta\}\}}{\epsilon_p\{U, \theta_*\}} \right] = \left(\frac{V_p\{v, \theta\}}{U} \right)^n \cdot f\{\theta_i\{v, \theta\}\} \tag{9}$$

where it will be recalled that the shape function $f\{\theta_i\} \equiv \epsilon_p\{V_p, \theta_i\}/\epsilon_p\{V_p, \theta_*\}$ describing the dependence of erosion yield on angle of incidence is normalized such that $f\{\theta_*\} = 1$. To complete the calculation of $E\{\theta, \ldots\}$ it remains to specify the three inertial impaction functions: $V_p\{v, \theta\}/U$, $\theta_i\{v, \theta\}/(\pi/2)$, and $\eta_{\text{local}}\{v, \theta\}$ (see the following subsection). Of particular interest to us will be the maximum local value $E_{\max}$ of E, occurring at angular position $\theta_{E_{\max}}$, as well as the mean value $\bar{E}$ of E over the upwind-facing surface of the circular cylinder, that is,

$$\bar{E} \equiv \left(\frac{2}{\pi}\right) \cdot \int_0^{\pi/2} E\{\theta, \ldots\} \cdot d\theta. \tag{10}$$

We should note at this point that $(ER)_{\text{ref}}$ (Eq. 1) scales as $U^{n+1} \cdot \phi_{p,\infty}$. Since our dimensionless E-functions are explicitly independent of $\phi_{p,\infty}$, this indicates that all *absolute erosion rates will be simply linearly proportional to the volume fraction of abrasive particles in the mainstream*, provided $\bar{v}$ and σ_g are kept constant, that is, $\phi_{p,\infty}$ is changed only due to changes in the mainstream *particle number density* (see the next section for a more general case). However, the dependence of erosion rates on mainstream velocity U will usually be more sensitive than U^{n+1} since the erosion rate functions E, $E_{\max}$, and $\bar{E}$ themselves contain an *implicit* dependence on U via the inertial impaction correlations described below. We will return to this interesting dependence in the next section and the subsection titled "'Direct' Use to Predict Erosion Behavior."

Inertial impaction on a cylindrical target in cross-flow; Stk_{eff} correlations

Defined as the ratio of the characteristic particle stopping time (t_p) and the flow time $t_{\text{flow}} = (d_t/2)/U$, the Stokes number, which dictates all impaction phenomena, is conventionally computed assuming the linear Stokes drag law. In an analysis of inertial impaction on spheres and cylinders in high-speed streams, Israel and Rosner (1983) introduced a generalized (effective) Stokes number, Stk_{eff}, which takes into account the non-Stokesian drag on the particles. It can be calculated in terms of conventionally defined Stokes number and particle Reynolds number (Re_p) via:

$$Stk_{\text{eff}} = Stk \cdot \psi\{Re_p\}. \tag{12}$$

The non-Stokes drag correction factor $\psi\{Re_p\}$ is defined by

$$\psi\{Re_p\} = \frac{24}{Re_p} \cdot \int_0^{Re_p} \frac{dRe'}{C_D\{Re'\}Re'} \tag{13}$$

and has the desired property $\psi \to 1$ when the drag coefficient $C_D \to 24/Re$ (Stokesian limit). A useful empirical approximation to extensive $C_D\{Re\}$ data for an isolated sphere, accurate up to $Re_p = O(10^3)$, is

$$C_D \cong \frac{24}{Re} \cdot [1 + 0.158(Re)^{2/3}]. \tag{14}$$

This representation leads to a correction factor ψ, which can be explicitly expressed in terms of Re_p as

$$\psi = \frac{3\left\{\sqrt{c}\, Re_p^{1/3} - \tan^{-1}\left\{\sqrt{c}\, Re_p^{1/3}\right\}\right\}}{c^{3/2} Re_p} \tag{15}$$

(see, e.g., Rosner and Tassopoulos, 1989). This convenient relation, with $c = 0.158$, has been used for all calculations reported here, as well as the construction of Figure 4 (with log-log coordinates). The integration over particle volume required to calculate the functions $E\{\theta, \ldots\}$, $E_{\max}$, and $\bar{E}$ will be carried out using the dimensionless particle volume variable $\xi \equiv v/v_{\text{crit}}$. However, all of the inertial impaction correlations (Israel and Rosner, 1983; Wang, 1986; Wessel and Righi, 1988; Konstandopoulos et al., 1993) for a cylinder in the cross-flow of a suspension of mono-sized particles are given below in terms of the effective Stokes number of Eq. 12, explicitly:

$$Stk_{\text{eff}} = \frac{1}{9} \cdot \frac{\rho_p U d_p^2}{\mu_g d_t} \cdot \psi\{U d_p/\nu\}. \tag{16}$$

When use is made of the result that the singular size $v_{\text{crit}} \equiv (\pi d_{p,\text{crit}}^3/6)$ corresponds to $Stk_{\text{eff,crit}} = 1/8$ (for a circular cylinder target at $Re_t^{1/2} \gg 1$), the algebraic (transcendental) (if it were not for the non-Stokesian correction $\psi\{Re_p\}$, the value of Stk_{eff} for particles large enough to remain in the continuum regime would simply be proportional to $\xi^{2/3}$ (i.e., projectile particle *surface area*)) relation between the variables Stk_{eff} and ξ is easily seen to be obtained from

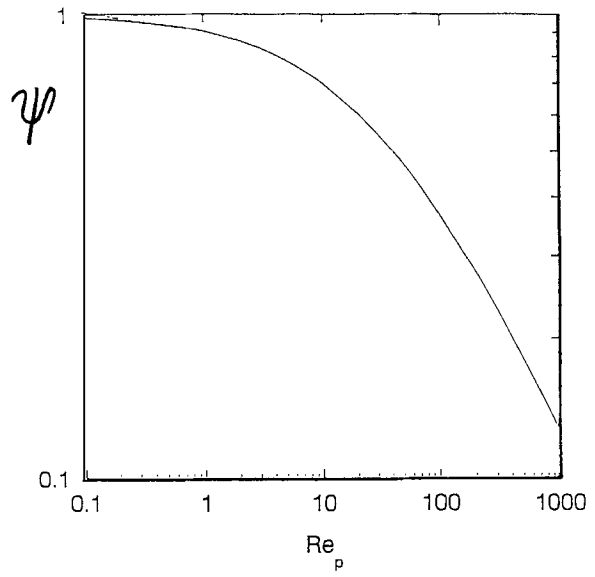

Figure 4. Double logarithmic plot of correction factor ψ for non-Stokesian particle drag (after Israel and Rosner, 1983).

$Stke_{\text{eff}} = Stk \cdot \psi\{Re_p\}$.

$$Stk_{\text{eff}} = \frac{1}{8} \cdot \xi^{1/3} \left\{ \frac{\sqrt{c}\, Re_{p,\text{crit}}^{1/3}\, \xi^{1/9} - \tan^{-1}\left(\sqrt{c}\, Re_{p,\text{crit}}^{1/3}\, \xi^{1/9}\right)}{\sqrt{c}\, Re_{p,\text{crit}}^{1/3} - \tan^{-1}\left(\sqrt{c}\, Re_{p,\text{crit}}^{1/3}\right)} \right\} \tag{17}$$

where $Re_{p,\text{crit}}$, the value of $Ud_{p,\text{crit}}/\nu_g$ (of order unity), will remain as an important parameter in all of the following calculations.

For a circular cylinder target in a cross-flow containing particles of a single specified size, the basic inertial impaction functions overall impingement efficiency (η_{cap}), the maximum angle experiencing impingement ($\theta_{\max}$), and the impact speeds at the forward stagnation point (V_{po}) and at the maximum angle experiencing impingement (V_{pm}) have been recalculated by numerical integration of the particle trajectory equations and the results correlated by Wessel and Righi (1988) using the notion of an effective Stokes number, Stk_{eff}, recommended by Israel and Rosner (1983). The correlation forms used are

$$\Gamma = \beta_1 \ln(8Stk_{\text{eff}}) + \beta_2\left(Stk_{\text{eff}} - \frac{1}{8}\right) + \beta_3\left(Stk_{\text{eff}} - \frac{1}{8}\right)^2 \tag{18}$$

or (cf. Israel and Rosner, 1983):

$$\Gamma = \left\{1 + \beta_1\left(Stk_{\text{eff}} - \frac{1}{8}\right)^{-1} + \beta_2\left(Stk_{\text{eff}} - \frac{1}{8}\right)^{-2} + \beta_3\left(Stk_{\text{eff}} - \frac{1}{8}\right)^{-3}\right\}^{-1} \tag{19}$$

where the recommended values for the coefficients appearing in these formulas are reproduced in Table 1. In addition, Wessel and Righi (1988) provide a set of correlations for local impingement efficiency ($\eta_{\text{local}}\{\theta\}$; cf. the previous subsection) at any angular position, θ, in terms of the overall impingement efficiency (η_{cap}) and the maximum angle experiencing impingement ($\theta_{\max}$):

$$\eta(\theta) \cong \frac{\pi}{2} \cdot \frac{\eta_{\text{cap}}}{\theta_{\max}} \cos\left(\frac{\pi}{2}\,\frac{\theta}{\theta_{\max}}\right). \tag{20}$$

The impact speed ($V_p\{\theta\}$) of a particle at any point ($\theta \le \theta_{\max}$) on the surface is correlated with the abovementioned values V_{pm}, V_{po}, and $\theta_{\max}$ by:

$$V_p\{\theta\} = -(V_{pm} - V_{po}) \cdot \cos\left(\frac{\pi}{2}\,\frac{\theta}{\theta_{\max}}\right) + V_{pm} \tag{21}$$

and, in our notation, $g(\upsilon, \theta) \equiv V_p/U$. The complement ($\alpha\{\theta\}$) of the angle of incidence (θ_i (Figure 1)) depends on the maximum angle experiencing impaction and an exponent, b, also correlated with Stk_{eff} by:

$$\frac{\alpha\{\theta\}}{(\pi/2)} = \left\{1 - \left(\frac{\theta}{\theta_{\max}}\right)^{1/b}\right\}^b \tag{22}$$

where:

$$b = 1 + \frac{\beta_1}{Stk_{\text{eff}}} + \frac{\beta_2}{Stk_{\text{eff}}^2} + \frac{\beta_3}{Stk_{\text{eff}}^3} \tag{23}$$

Table 1. Correlation Constants Used to Calculate Impacting Particle Target Efficiency, Impacting Angle (Figure 1), and Velocity (Wessel and Righi, 1988)

Correlation Parameter, Γ	Valid Stk_{eff} Range	Correlation Constants β_1	β_2	β_3	Correlation Equation
Target Efficiency, η_{cap}	$0.125 \rightarrow 0.5$	0.01978749	0.5136545	−0.0482858	Eq. 18
	> 0.5	1.54424	−0.538013	0.2020116	Eq. 19
Maximum angle experiencing impingement, $\theta_m/(\pi/2)$	$0.125 \rightarrow 0.5$	0.696596	−1.822407	1.1452745	Eq. 18
	> 0.5	0.7722744	−0.271871	0.06049905	Eq. 19
Impact velocity, $\lvert V_p\{0\}\rvert/U$	$0.125 \rightarrow 0.8$	0.0209863	0.8762208	−0.403482	Eq. 18
	> 0.8	1.038627	−0.327754	0.1115706	Eq. 19
Impact velocity, $\lvert V_p\{\theta_m\}\rvert/U$	$0.125 \rightarrow 0.5$	1.925045	−6.30525	3.796702	Eq. 18
	> 0.5	−0.242589	0.234317	−0.0446577	Eq. 19

where, according to Wessel and Righi, $\beta_1 = 0.1851488$, $\beta_2 = -0.0205901$, and $\beta_3 = 0.001530146$. Thus, in our present notation $h \equiv \theta_i/(\pi/2) = 1 - [\alpha(\theta)/(\pi/2)]$. In closing this section we note that compact correlations for η_{cap} and $V_p(\theta)/U$ have also been provided by Wang (1986); however, we have chosen not to "mix" correlations from different sources.

Abrasive particle size distribution in the mainstream

Using particle volume $v(=\pi d_p^3/6$ for a sphere of diameter $d_p)$ as the basic size variable, the normalized mainstream distribution function $C_\infty(v)$ appearing in subsection "Local and Total Erosion Rate Quadrature Expression" is defined such that the mainstream number density of particles with volume $v \pm (dv/2)$ is given by $N_p C_\infty(v)dv$, where N_p is the total particle number density. [In applications where the mainstream particles are *captured* by the target, the size distribution of *collected* particles can differ appreciably from $C_\infty(v)$ (see, e.g., Rosner et al., 1995)]. While the quadrature expression for the dimensionless erosion rate function $E(\theta, \ldots)$ admits *any* $C_\infty(v)$ of particular interest, all of the remaining calculations here will be based on the single-mode, two-parameter continuous distribution function:

$$C_\infty(v) = \frac{1}{v\sqrt{2\pi}\,\ln\,\sigma_g} \cdot \exp\left[-\frac{(\ln(v/v_g))^2}{2\ln^2\sigma_g}\right], \qquad (24)$$

which is said to be "log-normal" since $v \cdot C_\infty(v)$ is Gaussian in the volume variable ln v. Two particular values of the spread parameter σ_g will be of special interest: namely, the value $\sigma_g = 2.3$ (the corresponding distribution function in terms of particle diameter is also log-normal, but with the spread $\sigma_g = (2.3)^{1/3} = 1.32$), corresponding closely to "coagulation-aged" populations in the continuum regime (see, e.g., Friedlander, 1977; Rosner and Tassopoulos, 1989), and $\sigma_g = 1$, corresponding to the "mono-dispersed" (single-size) case. Rather than using the geometric mean particle volume v_g (at which $vC_\infty(v)$ maximizes) to characterize the average particle size in the population, we choose the number-mean volume defined by the integral of $vC_\infty(v)$ over all particle sizes in the population, that is,

$$\bar{v} \equiv \int_0^\infty vC_\infty(v)\,dv = v_g \cdot \exp\left(\frac{1}{2}\ln^2\sigma_g\right). \qquad (25)$$

As noted earlier, the product $\bar{v} \cdot N_p$ is the total *volume fraction* $\phi_{p,\infty}$ of the mainstream aerosol.

Instructive asymptotic limits

Two particularly important and instructive asymptotic limits are briefly considered here, namely, the limits $(\bar{v}/v_{crit})^{1/3} \gg 1$ or the ("monodispersed") limit $\sigma_g \to 1$. Both happen to be relevant to the "ideal" conditions for erosion yield tests, but we examine them here to provide a valuable check on our more general quadratures, and for the insight they provide.

The asymptotic limit $(\bar{v}/v_{crit})^{1/3} \gg 1$. In this limit most particles in the population are so large that they will follow nearly straight-line paths before impacting the circular cylinder at the velocity $V_p \approx U$ with angle of incidence $\theta_i \approx \theta$ (see Figure 1). In terms of the inertial impaction functions introduced in the previous subsection we see that, in this limit:

$$\eta_{local}(v, \theta) \to \cos\,\theta \qquad (26)$$

$$\theta_{max} \to \pi/2 \qquad (27)$$

$$g(\equiv V_p(v, \theta)/U) \to 1 \qquad (28)$$

$$h(\equiv \theta_i/(\pi/2)) \to \theta/(\pi/2). \qquad (29)$$

Inspection of the quadrature expression $E(\theta, \ldots)$ (Eq. 8) reveals that when $(\bar{v}/v_{crit})^{1/3} \gg 1$ we should expect:

$$\lim_{(\bar{v}/v_{crit})^{1/3} \gg 1} E(\theta, \ldots) = \cos(\theta) \cdot f(\theta), \qquad (30)$$

irrespective of σ_g and $Re_{p,crit}$, of course, irrespective of the erosion yield parameter f_0, θ_*, or n. This limit will therefore be included on several of the summary graphs shown in the next section. As one important consequence of Eq. 30 (another interesting corollary of Eq. 30 is that $\mathrm{Lim}_{(\bar{v}/v_{crit})^{1/3} \gg 1}(dE/d\theta)_{\theta=0} = (df/d\theta)_{\theta=0}$, which, in general, is a positive number (Figures 2, 3); as discussed in subsection "Examination of Approximations," this implies that *erosion will "sharpen" the nose of initially blunt metal objects*), we see that the stagnation point value $E(0, \ldots)$ cannot exceed the abovementioned parameter $f(0)$.

The "single particle size" asymptotic limit ($\sigma_g \to 1$). In the limit of vanishing particle population spread, corresponding in our notation to $\sigma_g \to 1$, the distribution function $C_\infty(v)$ becomes Dirac-like and all particles in the population will have a single volume, necessarily equal to the number-mean volume $\bar{v}$. Then, in our calculation of "total" local erosion rate ("Local and Total Erosion Rate Quadrature Expression") no integration over particle volume is necessary and we are led immediately to the interesting result:

$$\lim_{\sigma_g \to 1} E(\theta, \ldots) = f\theta_i(\bar{v}, \theta)g^n(\bar{v}, \theta)\eta_{local}(\bar{v}, \theta), \qquad (31)$$

which involves each of the abovementioned inertial impaction correlation functions $\theta_i/(\pi/2)$, g, and η_{local}, but all evaluated for the single particle size $\bar{v}(> v_{crit})$ in the prevailing environment. This result, which is formally valid for any $\bar{v}/v_{crit}$, and any value of the dimensionless parameters $\mathrm{Re}_{p,crit}$, f_0, θ_*, n, will also be shown in several of the graphs presented in the following section (e.g., Figure 5).

Results and Discussion

For the log-normal distribution C_∞ and the erosion yield law, local impingement angle and efficiencies, as discussed in the preceding section, we define and calculate below a dimensionless local erosion rate function, $E(\theta)$, as:

$$E(\theta) = \frac{1}{\bar{v}} \cdot \int_0^\infty v \cdot \eta_{local}(v, \theta)C_\infty(v)g^n(v, \theta)f\left(h(v, \theta)\frac{\pi}{2}\right)dv. \qquad (32)$$

The dimensionless functions f, g, and η_{local} appearing in the integrand and discussed in the previous section are evaluated using the relation (discussed in the previous section) between effective Stokes number, Stk_{eff}, and dimensionless particle volume, $\xi(\equiv v/v_{\text{crit}}$, where v_{crit} is the "critical" volume (the volume of the smallest particle capable of inertial impaction on the target in prevailing environment) and $Re_{p,\text{crit}}$, the Reynolds number based on mainstream velocity, diameter of the critical size particle, and, in the Stokesian limit ($Re_{p,\text{crit}} \to 0$), one sees that $Stk_{\text{eff}} \to (1/8)\cdot\xi^{2/3}$. The dimensionless erosion rate function defined by Eq. 32, for rapid estimation, has been calculated using a *finite-analytic* scheme in which we divide the size spectrum into a number of sections. In each section k ($k = 1, 2, 3, \ldots, M$) we estimate the parameters A_k and q_k such that they best-fit the local power law: $\eta_{\text{local}}(\theta, v)\cdot g^n(\theta, v)\cdot f(h(\theta, v)\pi/2) \equiv A_k v^{q_k}$. The integration in Eqs. 5 and 32 is then done piecewise using the following closed-form relation (Rosner and Tassopoulos, 1989) for the "partial moments" of $C(v)$:

$$\int_\alpha^\beta v^q C(v)\,dv = \frac{1}{2}\exp\left[q\ln v_g + \frac{1}{2}q^2\ln\sigma_g\right] \cdot\left\{\text{erf}\left[\frac{\ln\left(\frac{\beta}{v_g}\exp\left(-q\ln^2\sigma_g\right)\right)}{\sqrt{2}\ln\sigma_g}\right] - \text{erf}\left[\frac{\ln\left(\frac{\alpha}{v_g}\exp\left(-q\ln^2\sigma_g\right)\right)}{\sqrt{2}\ln\sigma_g}\right]\right\} \quad (33)$$

In Figure 5, we show the polar plot of dimensionless erosion rate on the upwind side of the cylinder for the population spread $\sigma_g = 2.3$ (the "self-preserving" value for Brownian coagulation in the continuum regime). The plot is shown for different values of dimensionless mean volume, $\bar{\xi}$, defined as the ratio of $\bar{v}$ of the mainstream distribution and the critical volume, v_{crit}. The increase in the mean volume (size) increases the inertial impacting ability of the particles in the mainstream, leading to the increase in the erosion rate observed. Also shown on the plot is the product function $f(\theta)\cos\theta$; that is, the asymptotic value of the dimensionless erosion rate function, $E(\theta)$, in the limit of very large Stokes number. The angle θ on the cylinder where the maximum erosion rate takes place also increases and asymptotically approaches the value of θ for which $f(\theta)\cos(\theta)$ is maximum (here $\theta = 46.4°$), as has been discussed in the preceding subsection. We have reported the preceding results for typical values of the remaining parameters encountered in practical situations: $n = 2.5$, $\theta_* = 66°$, $f_0 = 0.28$. In Figures 6–20, we display the sensitivity to the parameters σ_g, n, f_0, θ_*, and $Re_{p,\text{crit}}$ of the average and maximum dimensionless erosion rate, $\bar{E}$ and $E_{\max}$, and the position, $\theta_{E_{\max}}$, where the maximum erosion rate occurs. In Figures 6 and 16 we show the dependence of the average and maximum erosion rates on the dimensionless mean particle diameter, $\bar{\xi}^{1/3}$, for different

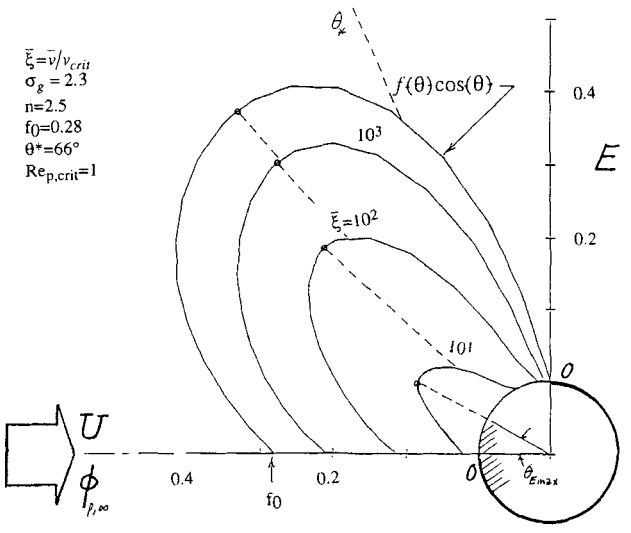

Figure 5. Polar plot of dimensionless erosion rate function $E(\theta, \ldots)$ (Eq. 8) at several values of $\bar{v}/v_{\text{crit}}$.
Case shown: $Re_{p,\text{crit}} = 1$, $\sigma_g = 2.3$, $n = 2.5$, $f(0) = 0.28$, $\theta_* = 66°$.

values of population spread parameter, σ_g. Increase in the standard deviation of the particle distribution in the mainstream (for a given number-mean size (volume)) results in particles of larger sizes impacting the target, resulting in higher erosion rate. Also shown on these graphs are the maximum and average values of the function $f(v)g^n(v)h(v)$, which corresponds to the asymptotic behavior of $E(\theta)$ in the limit of $\sigma_g = 1$, that is, all particles in the mainstream have the same size, $\bar{v}$, Eq. 31. We present our results for the dimensionless mean particle *diameter*, $\bar{\xi}^{1/3}$, between 1 and 10.

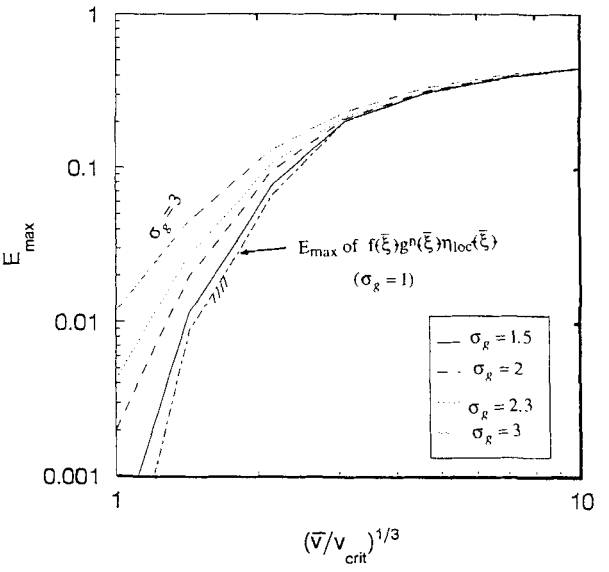

Figure 6. $E_{\max}$ as function of the particle size parameter $(\bar{v}/v_{\text{crit}})^{1/3}$ for values of the population spread σ_g.
Case shown: $Re_{p,\text{crit}} = 1$, $n = 2.5$, $f(0) = 0.28$, $\theta_* = 66°$.

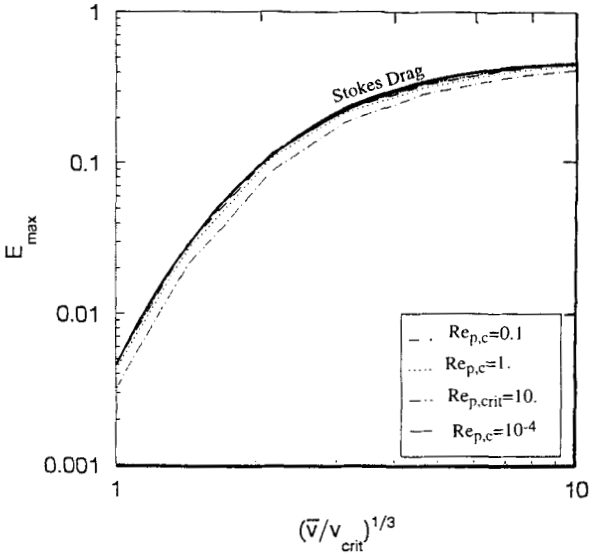

Figure 7. E_{max} as function of the particle size parameter $(\bar{v}/v_{crit})^{1/3}$ for values of the particle Reynolds number $Re_{p,crit}$.

Case shown: $\sigma_g = 2.3$, $n = 2.5$, $f(0) = 0.28$, $\theta_* = 66°$.

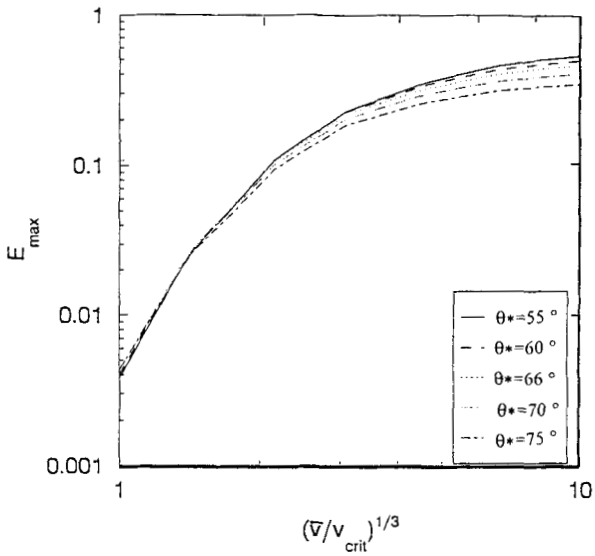

Figure 9. E_{max} as function of the particle size parameter $(\bar{v}/v_{crit})^{1/3}$ for values of the singular incidence angle θ_*.

Case shown: $Re_{p,crit} = 1$, $\sigma_g = 2.3$, $n = 2.5$, $f(0) = 0.28$.

The maximum and average erosion rates are observed to approach the asymptotic values of $f(\theta)\cdot\cos(\theta)$ (high Stokes number limit) for $\bar{\xi}^{1/3} = 10$. For metal targets the most vulnerable erosion angle of incidence, θ_*, is often found to lie between 60 and 70 degrees (see, e.g., Tabakoff et al., 1980). We have investigated the effect of the parameter θ_* (between 55 and 75 degrees) on the erosion rates and find that the erosion rates decrease as θ_* increases (Figures 9, 19, 24). In Figures 7 and 17, we show the dependence of the erosion rates on the critical particle "slip" Reynolds number. A particle Reynolds number of zero corresponds to the case of Stokesian drag and, using these figures, one can avoid the systematic error that would be made in estimating the erosion rates based on the (simplifying but erroneous) assumption that suspended particle drag follows Stokes law. An increase in the value of f_0 (i.e., erosion propensity at normal incidence) increases the values of $f(\theta)$ for $\theta < \theta_*$ (Figure 3), and thereby increases the local, maximum, and average erosion rates (Figures 10 and 20). Indeed, as shown in the previous subsection, f_0 is the limiting value of E at the forward stagnation point $(\bar{v}/v_{crit})^{1/3} \gg 1$).

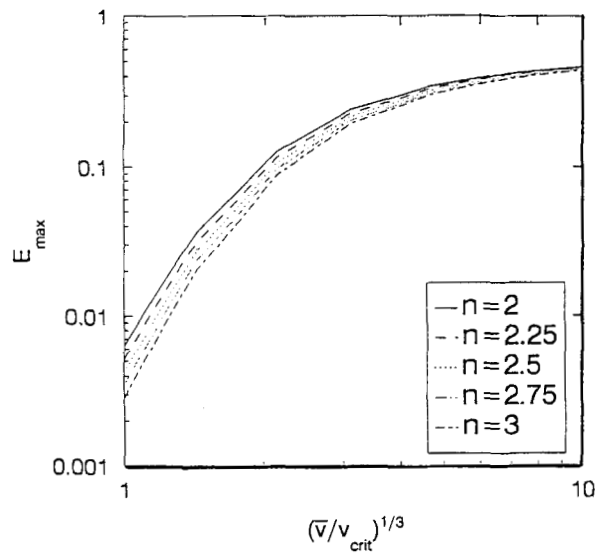

Figure 8. E_{max} as function of the particle size parameter $(\bar{v}/v_{crit})^{1/3}$ for several values of velocity exponent n.

Case shown: $Re_{p,crit} = 1$, $\sigma_g = 2.3$, $f(0) = 0.28$, $\theta_* = 66°$.

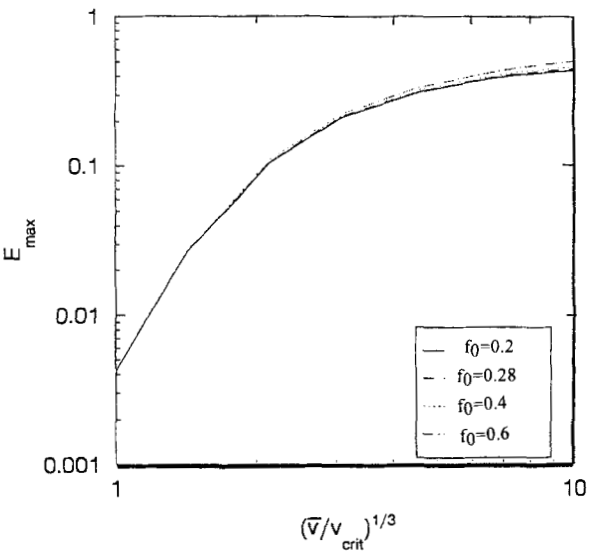

Figure 10. E_{max} as function of the particle size parameter $(\bar{v}/v_{crit})^{1/3}$ for values of $f(0)$.

Case shown: $Re_{p,crit} = 1$, $\sigma_g = 2.3$, $n = 2.5$, $\theta_* = 0.66°$.

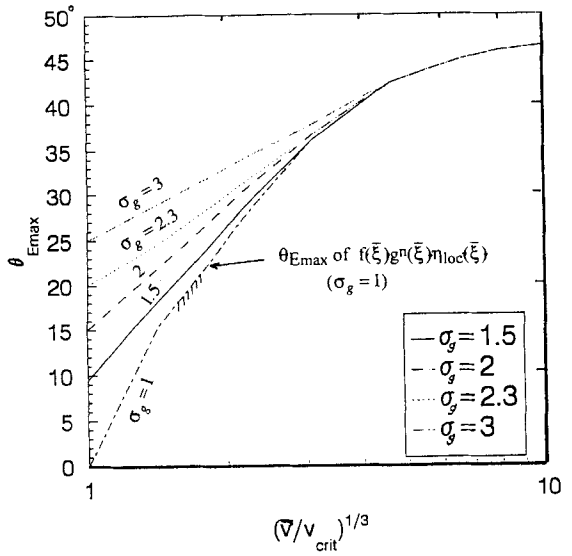

Figure 11. $\theta_{E_{max}}$ as function of the particle size parameter $(\bar{v}/v_{crit})^{1/3}$ for values of the population spread σ_g.

Case shown: $Re_{p,crit} = 1$, $n = 2.5$, $f(0) = 0.28$, $\theta_* = 66°$.

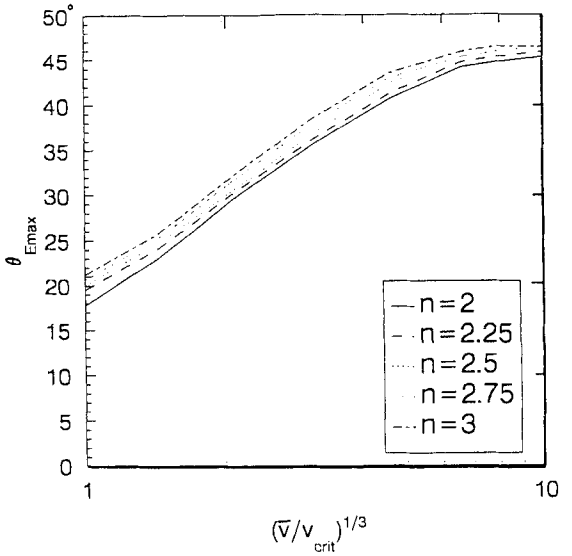

Figure 13. $\theta_{E_{max}}$ as function of the particle size parameter $(\bar{v}/v_{crit})^{1/3}$ for values of velocity exponent n.

Case shown: $Re_{p,crit} = 1$, $\sigma_g = 2.3$, $f(0) = 0.28$, $\theta_* = 66°$.

The angle, $\theta_{E_{max}}$, at which the maximum erosion rate takes place increases with increasing mean particle diameter (see, e.g., Figure 5) provided f_0 is sufficiently small. These $\theta_{E_{max}}$-values asymptotically reach the value of θ for which $f(\theta) \cdot \cos\theta$ is maximum. However, it is noteworthy that the approach is nonmonotonic at sufficiently high f_0 values (see Figure 15).

Our results can be used to calculate the local *sensitivity* of the erosion rate to parameters of particular interest, for example, mainstream velocity. In this case we can calculate the local *exponent* $\partial \ln (\overline{ER})/\partial (\ln U)$, taking into account the implicit dependence of, say, $E(\theta)$ on U via v_{crit} and $Re_{p,crit}$. Our result,

$$n_{eff} + 1 \equiv \frac{\partial \ln (\overline{ER})}{\partial \ln U} = n + 1 + \frac{1}{2}\left(1 + \frac{\partial \ln \psi}{\partial \ln Re_{p,c}}\right)\left(\frac{\partial \ln (\bar{E})}{\partial \ln \bar{\xi}^{1/3}} - \frac{\partial \ln (\bar{E})}{\partial \ln Re_{p,c}}\right) \quad (34)$$

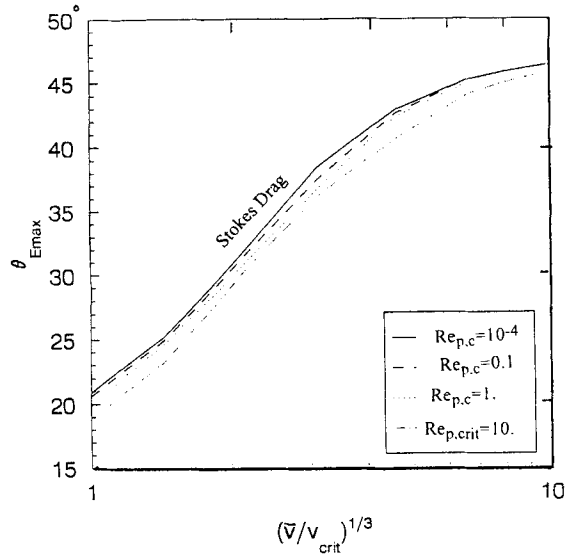

Figure 12. $\theta_{E_{max}}$ as function of the particle size parameter $(\bar{v}/v_{crit})^{1/3}$ for values of the particle Reynolds number $Re_{p,crit}$.

Case shown: $\sigma_g = 2.3$, $n = 2.5$, $f(0) = 0.28$, $\theta_* = 66°$.

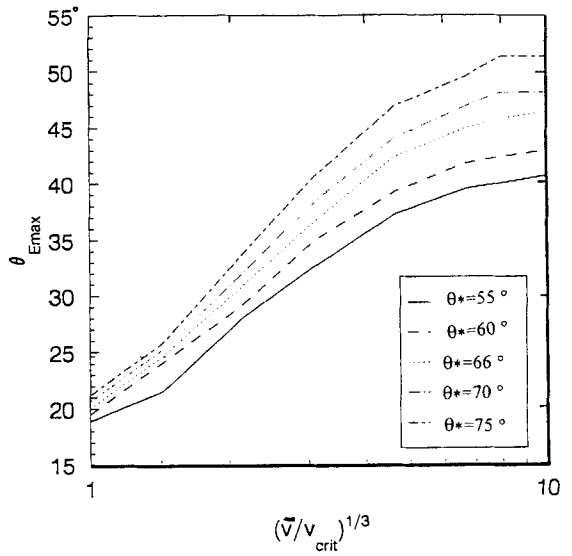

Figure 14. $\theta_{E_{max}}$ as function of the particle size parameter $(\bar{v}/v_{crit})^{1/3}$ for values of the singular incidence angle θ_*.

Case shown: $Re_{p,crit} = 1$, $\sigma_g = 2.3$, $n = 2.5$, $f(0) = 0.28$.

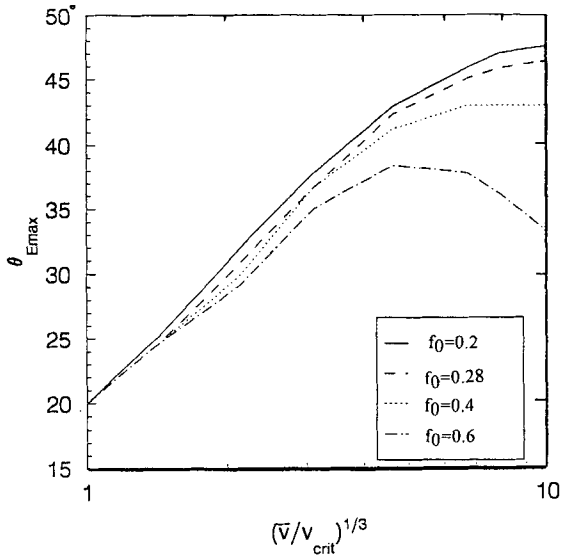

Figure 15. $\theta_{E_{max}}$ as function of the particle size parameter $(\bar{v}/v_{crit})^{1/3}$ for values of $f(0)$.

Case shown: $Re_{p,crit} = 1$, $\sigma_g = 2.3$, $n = 2.5$, $\theta_* = 66°$.

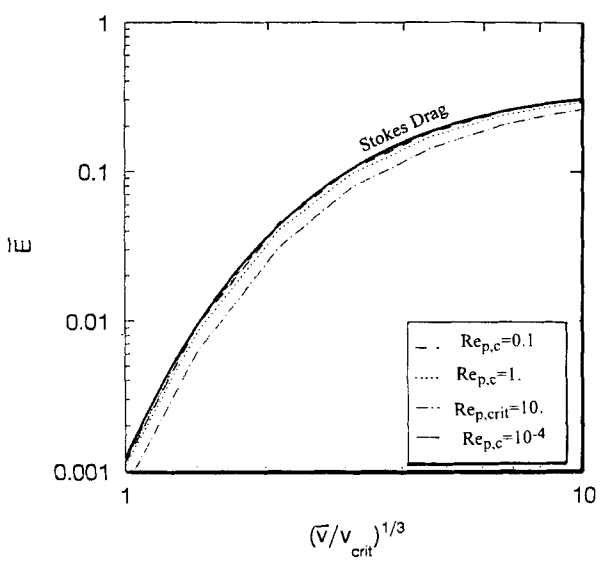

Figure 17. $\bar{E}$ as function of the particle size parameter $(\bar{v}/v_{crit})^{1/3}$ for values of the particle Reynolds number $Re_{p,crit}$.

Case shown: $\sigma_g = 2.3$, $n = 2.5$, $f(0) = 0.28$, $\theta_* = 66°$.

reveals that this exponent can exceed $n+1$ by an appreciable amount due to the term involving the indicated logarithmic derivatives (this is the reason why we have displayed Figures 4 and 6–20 with logarithmic scales; incidentally, Eq. 34 (and Eqs. 36, 39) is also valid for the maximum erosion rate, E_{max}, provided the appropriate graph for (log) E_{max} vs. (log) $(\bar{v}/v_{crit})^{1/3}$ is used). Estimating these derivatives from Figures 4 and 17, respectively, for our illustrative case (see the next subsection) reveals that, whereas $n+1 = 3.5$, $\partial\,[\ln(\overline{ER})/\partial \ln U] \approx 6$ under these particular conditions. Of course, both exponents are large and indicate that a reduction in mainstream velocity will dramatically reduce erosion rates.

Another interesting corollary of this steep dependence of erosion rate on U is that if the mainstream is fluctuating (with a frequency perhaps up to but not far exceeding $1/t_{p,crit}$), then the time-average erosion rate will be systematically larger than the erosion rate evaluated at the time-average velocity by the approximate factor:

$$1 + \frac{n_{eff}(n_{eff}+1)}{2} \cdot \frac{\overline{(U-\bar{U})^2}}{\bar{U}^2}, \qquad (35)$$

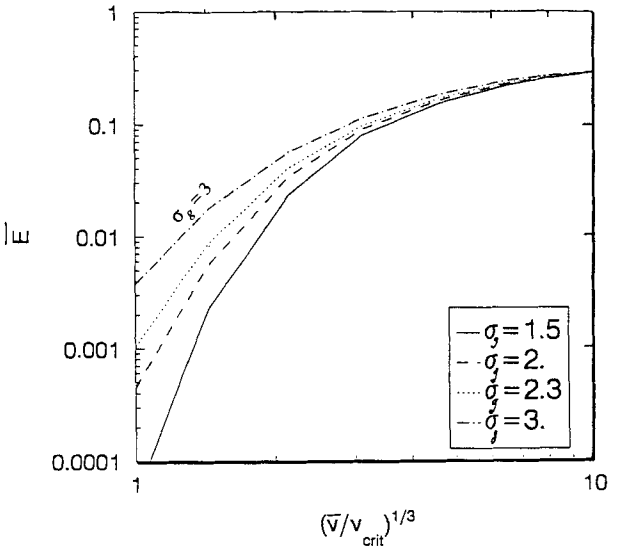

Figure 16. $\bar{E}$ as function of the particle size parameter $(\bar{v}/v_{crit})^{1/3}$ for several values of the population spread σ_g.

Case shown: $Re_{p,crit} = 1$, $n = 2.5$, $f(0) = 0.28$, $\theta_* = 66°$.

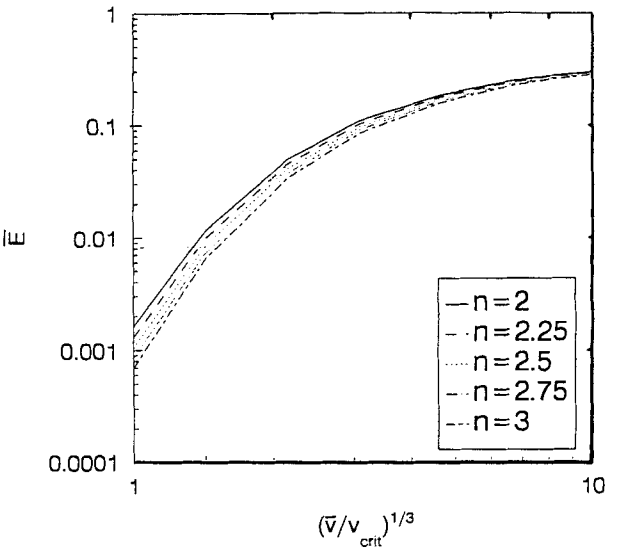

Figure 18. $\bar{E}$ as function of the particle size parameter $(\bar{v}/v_{crit})^{1/3}$ for values of velocity exponent n.

Case shown: $Re_{p,crit} = 1$, $\sigma_g = 2.3$, $f(0) = 0.28$, $\theta_* = 66°$.

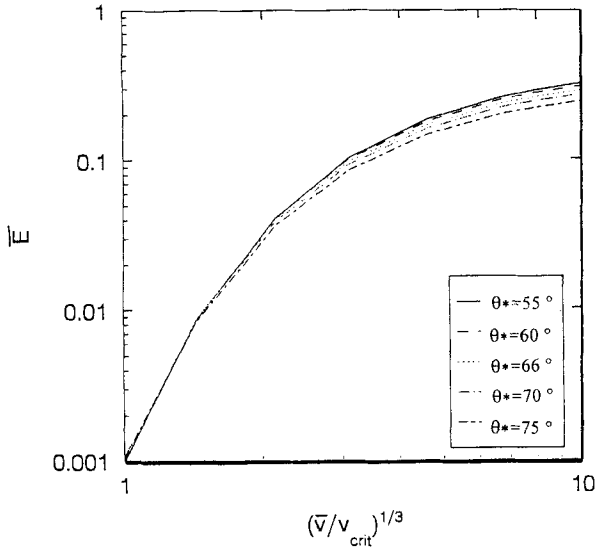

Figure 19. $\bar{E}$ as function of the particle size parameter $(\bar{v}/v_{crit})^{1/3}$ for values of the singular incidence angle θ_*.

Case shown: $Re_{p,crit} = 1$, $\sigma_g = 2.3$, $n = 2.5$, $f(0) = 0.28$.

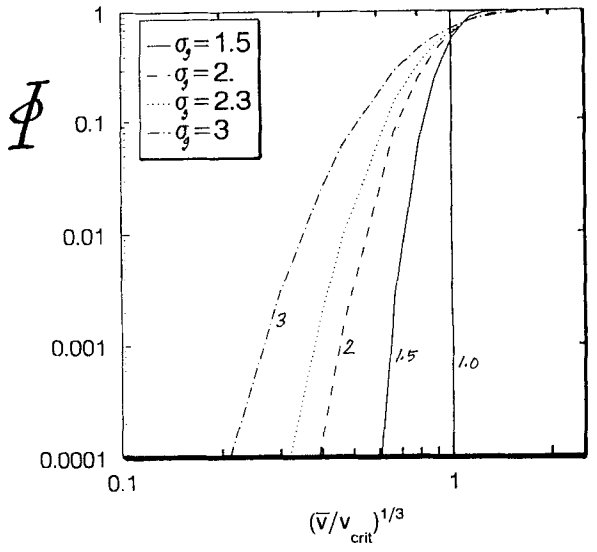

Figure 21. Fraction Φ of the total volume $\phi_{p,\infty}$, which is supercritical (capable of inertial impaction) in the prevailing environment.

Log-normal $C_\infty(v)$.

which can be appreciable even at modest "turbulence intensities"; for example, at 50% turbulence intensity this factor is about 5 (rather than 2.1 based on $n_{eff} = n$).

Also of interest is the sensitivity of erosion rate to the volume fraction $\phi_{p,\infty}$ of suspended abrasive particles. If $\phi_{p,\infty}$ is changed only because of a change in *particle number density* at constant $\bar{v}$, then it is readily shown that $\partial \ln (\overline{ER})/\partial \ln \phi_{p,\infty}$ is unity, that is, erosion rates will depend linearly on *mainstream particle number density*. However, if the change in $\phi_{p,\infty}$ were instead entirely due to the change in $\bar{v}$ (at constant N_p), then one finds the larger exponent:

$$\left(\frac{\partial \ln \overline{ER}}{\partial \ln \phi_{p,\infty}}\right)_{N_p = \text{const}} = 1 + \frac{1}{3}\left(\frac{\partial \ln \bar{E}}{\partial \ln \bar{\xi}^{1/3}}\right). \tag{36}$$

We note that this is *not* merely the result of increasing the volume-weighted frequency of abrasive particle impacts, a "plausible" hypothesis that would have led instead to the exponent:

$$1 + \frac{1}{3}\frac{\partial \ln \Phi}{\partial \ln \bar{\xi}^{1/3}} \tag{37}$$

where Φ is the fraction of $\phi_{p,\infty}$, which is "supercritical" (capable of impacting), that is,

$$\Phi = \frac{1}{\bar{v}} \cdot \int_{v_{crit}}^{\infty} v C_\infty(v)\, dv \tag{38}$$

(shown plotted in Figure 21, again using log-log scales). Thus, the sensitivity $\partial \ln \overline{ER}/\partial \ln \phi_{p,\infty}$ will be between unity and Eq. 36, depending on what fraction of the change in $\phi_{p,\infty}$ is associated with a change in mean particle volume $\bar{v}$.

Also of practical interest is the predicted sensitivity of erosion rate to *target* diameter (or twice the nose radius of a turbine bladelike shape; see subsection "Generalizations"). In this case one finds

$$\frac{\partial \ln \overline{ER}}{\partial \ln d_t} = -\frac{\frac{1}{2}\left(\frac{\partial \ln \bar{E}}{\partial \ln \bar{\xi}^{1/3}}\right)}{1 + \frac{1}{2}\frac{\partial \ln \psi}{\partial \ln Re_{p,c}}}. \tag{39}$$

One sees that this local exponent is always negative and only vanishes in the limit $(\bar{v}/v_{crit})^{1/3} \to \infty$. Moreover, the sensitivity

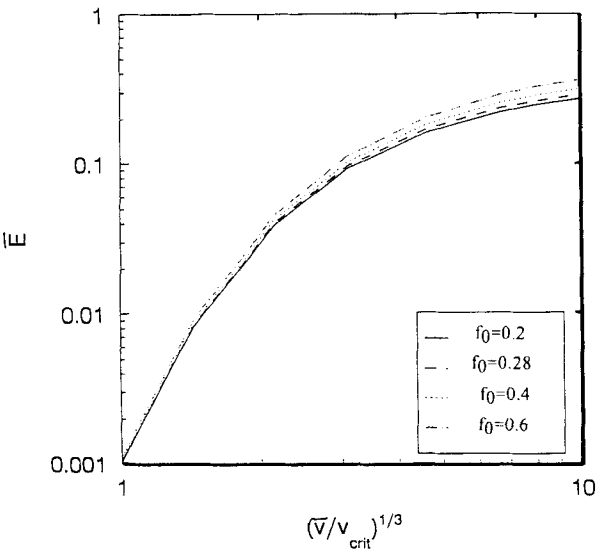

Figure 20. $\bar{E}$ as function of the particle size parameter $(\bar{v}/v_{crit})^{1/3}$ for values of $f(0)$.

Case shown: $Re_{p,crit} = 1$, $\sigma_g = 2.3$, $n = 2.5$, $\theta_* = 66°$.

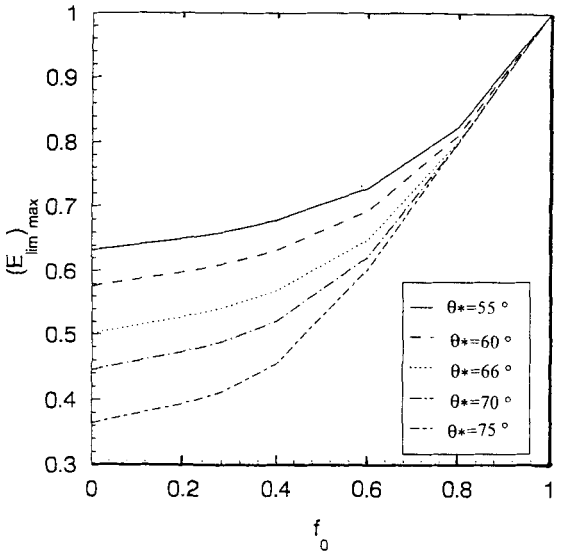

Figure 22. Maximum value of E in the limit of infinite Stokes number; effect of the erosion yield parameters f_0 and θ_*.

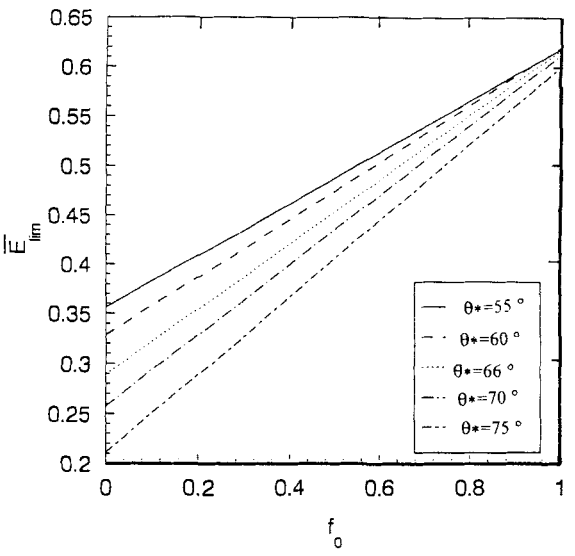

Figure 24. Average erosion rate function $\bar{E}$ (upwind-facing area) in the limit of infinite Stokes number; effect of the erosion yield parameters f_0 and θ_*.

of erosion rate to target diameter increases somewhat as a result of the non-Stokesian drag correction (cf. Figure 4). These results could be useful for evaluating the benefits/costs of the strategy of adopting larger target nose radius to reduce erosion rates in a more "ruggedized" boiler or turbine design.

Finally, because of the theoretical and practical importance of the large Stokes number limit ($(\bar{v}/v_{crit})^{1/3} \gg 1$) we collect, in Figures 22, 23, and 24, the pertinent limiting results for E_{max}, $\theta_{E_{max}}$, and $\bar{E}$ over the range of parameters θ_* and f_0 (Figures 2 and 3) of practical interest. Not surprisingly, erosion rates become rather insensitive to θ_* (Figure 22) when the relative erosion propensity at normal incidence, f_0, is large (say, above 0.8). It is also noteworthy that in the high Stokes number limit, mean erosion rates scale linearly with f_0 over the entire θ_* range of interest (Figure 24).

Considering the fundamental simplicity of our mathematical model/formulation of the particle impact erosion problem (see the section on the mathematical model), the above-mentioned results are seen to provide a remarkable amount of insight into the dependence of erosion rates on both environmental and phenomenological materials parameters. Further applications and extensions of this model are taken up in the next section.

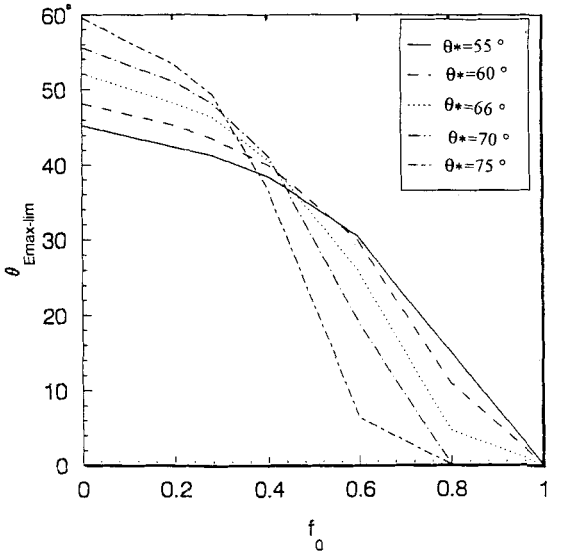

Figure 23. Angular position of maximum erosion rate in the limit of infinite Stokes number; effect of the erosion yield parameters f_0 and θ_*.

Implications, Applications, and Generalizations

"Direct" use to predict erosion behavior

It is straightforward to use the results of the preceding section to predict local and average erosion rates in many particular environments of practical interest. This can be briefly illustrated (for a concise summary of "best-fit" values of $\epsilon_p\{V_{p,ref} = 10^2 \text{m/s}, \theta_*\}$, n, θ_*, and f_0 based on erosion test rig data in the open literature, see Kho et al. (1994) (for targets of sufficient ductility to exhibit θ_*-values in the range considered here)) using the Kingston coal ash/304 stainless steel erosion yield parameters mentioned in the subsection on the erosion yield law, along with the environmental conditions considered in chapter 8 of Rosner (1986, 1990), namely, $U = 10$ m/s, $d_{p,crit} \approx 14$ μm, $\overline{d_p} = 20$ μm, $d_t = 5$ cm with a suspended particle mass fraction of 10^{-2} and the log-normal parameter σ_g of about 2.3. With these numbers we readily find $(\bar{v}/v_{crit})^{1/3} \approx 1.43$, $Re_{p,crit} \approx 0.6$, $\epsilon_p\{U, \theta_*\} = 0.98 \times 10^{-7}$, $(\bar{v}N_pU)_\infty \approx 8.26$ μm/s, $(ER)_{ref} \approx 37$ μm/y, $(E)_{max} \approx 0.028$, $\langle E \rangle \approx 0.0084$, $(ER)_{max} \approx 1$ μm/y, $\theta(ER)_{max} \approx 24.6°$, and $\langle ER \rangle \approx 0.3$ μm/y. These particular results indicate quite

modest erosion damage over the projected lifetime of the power plant; however, if the results of similar calculations predicted erosion rates considered to be intolerable, one might then investigate the costs/benefits of the following options: reduce local gas velocities, reduce fly-ash burden (by combustor configuration or ash content of coal), and/or consider the cost/feasibility of specifying metal alloys more wear-resistant than #304 stainless steel.

"Indirect" use to infer parameters in the erosion yield law

Inspection of our "universal" results (preceding section) reveals that $(ER)_{\text{ref}}$ and/or the calculated quantities E, $E_{\max}$, $\theta_{E_{\max}}$, and/or $\langle \overline{E} \rangle$ are sometimes sensitive to the parameters θ_*, f_0, and n appearing in the erosion yield law. In these regimes an "observation" of any or all of these quantities for a cylinder in a "known" test environment can clearly be used to extract rational estimates of those parameters that are least well known—for example, θ_* and/or f_0 for a material never previously studied in a well-characterized erosion test rig. This might be a reasonable provisional method for making extrapolations to related environmental conditions, including ultimately predicting erosion damage on more complex shapes (e.g., a turbine blade) by particle trajectory analysis.

Examination of approximations

Confidence in the validity of most if not all of our underlying assumptions can be generated based on the sequential observations below. However, in some cases we are led to interesting questions that appear to remain open and will warrant and, hopefully, motivate a closer examination in follow-on research. Generalizations that relax one or more of these assumptions are postponed to the following subsection.

A1. Validity of high Re, point-particle trajectory calculations for a circular cylinder in cross-flow. For conditions representative of, say, an "unshielded" boiler tube exposed to coal-ash-laden combustion products, the principal assumptions underlying the impaction calculations/correlations are quite accurate. This is because the tube Reynolds number ($O(4\times 10^3)$; see, e.g., Rosner, 1986, Chap. 8) is usually high enough for boundary layer corrections (to $Stk_{\text{eff,crit}}$ and local particle trajectories near the upwind-facing surfaces) to be negligible (see, also, Menguturk and Günes, 1984, and Rosner and Fernandez de la Mora, 1984), and those particles large enough to impact with velocities of order U will indeed exhibit negligible Brownian motion (Fernandez de la Mora and Rosner, 1982), and yet remain negligibly small on the scale of the tube diameter ($d_p/d_t = O\{10^{-4}\}$).

Several further simplifications underlie the inertial impaction correlations we have exploited, for example, the $\cos((\theta/\theta_{\max})\pi/2)$ angular dependence of local particle impingement flux at *all* supercritical Stokes numbers and at particle slip Reynolds number outside the domain of Stokes drag law. The accuracy of this $\cos((\theta/\theta_{\max})\pi/2)$ representation can be judged by consulting the particle trajectory numerical calculations of Brun et al. (1953, 1955) and Wessel and Righi (1988).

The correlation-predicted values of the abovementioned local functions were calculated and compared to the values for those quantities obtained by Wessel and Righi (1988) from actual particle trajectory integrations. Consistent with the comments made by Wessel and Righi (1988), we found that there are significant deviations between the correlation function values and those obtained from specific trajectory calculations, especially when $Stk_{\text{eff}} < 0.5$. As might be expected, these discrepancies are most noticeable in the evaluation of the local (cf. integrated) properties. For example, when Stk_{eff} is 0.25, the local impingement efficiency as calculated from the correlation is approximately 75% higher than that from trajectory calculation. Fortunately, this discrepancy decreases to about 26% for $Stk_{\text{eff}} = 0.5$ and to 4% for $Stk_{\text{eff}} = 4$, and one would expect that very low Stk_{eff}-particles (near-critical size) account for only a small fraction of the total erosion.

A2. Success of the effective Stokes number concept in the domain of non-Stokes particle drag. The success of the "effective Stokes number" concept for Re_p-values up to as high as 10^3 has been demonstrated for *impacting particle capture fractions* (for $s = 1$) by Israel and Rosner (1983). Their recommendation that this simple technique would also correlate *impaction velocities* and *angles* was later confirmed by Wang (1986), and again by Wessel and Righi (1988), especially in the domain away from the immediate vicinity of $Stk_{\text{eff,crit}}$, for example, $Stk_{\text{eff}} \geq 0.5$, where most erosion damage is likely to occur (because of the sensitivity of erosion yield to impact velocity). This is quite encouraging since Re_p-values in many two-phase flow engineering applications (Rosner and Tandon, 1995a), including the present class of applications, will require these systematic non-Stokesian drag corrections (cf. the Re_p-effects displayed in Figures 7, 12, and 17).

A3. Engineering applicability of available erosion yield data $(\epsilon_p\{V_p, \theta_i\})$. It is worth explicitly noting that most erosion rate "predictions" for, say, boiler and combustion turbine applications have been based on the premise that erosion yield data can be invoked in situations where particles actually arrive simultaneously over a wide "band" of velocities and angles of incidence. Indeed, this premise underlies the development/use of such erosion test rigs (see, e.g., Finnie, 1959; Tabakoff et al., 1979a,b). However, if the erosion mass loss process is not simply a "single impact" phenomenon this (usually implicit) "additivity" or "uncoupling" assumption should probably be examined more critically, perhaps based on the erosion rate experiments involving, for example, "pairs" of incidence angles. We are currently unaware of such experimental tests of "additivity" in erosion situations.

Another type of coupling phenomenon, which apparently has not been systematically studied, is the possible "protective" effect of the simultaneous *acquisition* of much smaller particles (or even condensed vapor) on the component whose erosion is of concern (see, also, A4 below). In such cases the erosion yield law would have to be enlarged to include the prevailing average inventory (quasi-steady coverage) of the semiprotective layer, and the nature of this dependence would have to be studied experimentally, and/or, perhaps, theoretically (Konstandopoulos and Rosner, 1995; Rosner et al., 1992).

A4. Neglect of particle-particle interactions and "rebound" phenomena. In most of the applications of concern here the *volume fraction* of suspended particles, $\phi_{p,\infty}$, is small enough (usually of order 10^{-6}) to render particle-particle interaction effects in the vicinity of the target negligible. Indeed, if one views the particle "flow field" as if there were no carrier gas

(e.g., consider the limit $Stk \to \infty$, with elastic rebound from the cylinder) this "particle gas flow" past the cylinder would correspond to a Knudsen number (ratio of mean-free-path to target diameter) of the order of $(2/3)(\phi_p)^{-1} \cdot (d_p/d_t)$, which is about 2×10^2 for our present numerical example (see the subsection titled "'Direct' Use to Predict Erosion Behavior"). This value is large enough to justify the assumption of "free-particle" flow.

On the issue of erosion due to *rebounding* particles (e.g., accounting for multiple impacts on the same target) it should be realized that the combination of loss of particle velocity due to "inelasticity" and the sensitivity of erosion yield to impact velocity conspire to make successive collisions comparatively ineffective, suggesting the engineering utility of a "single impact" erosion rate theory. This is in contrast to the situation for rebound effects on *particle capture*, which can be seen from the interesting study of Wang (1986). However, in this connection it is interesting to note that, in general, a target exposed to a stream containing a broad distribution of mainstream particle sizes will inevitably tend to *capture* the smallest particles under conditions in which the large suspended particles will be capable of rebound and/or erosion. This means that even at low suspension volume fractions, *particle-particle interactions at the surface cannot* be ruled out, depending on the relative arrival rates of "depositing" and "rebounding" particles. In fact, in many such situations the erosion yield (for the underlying material) would depend on the steady-state "coverage" (inventory) of the smaller (cushioning) particles (see also A3). A variant of this interesting situation (combined deposition and erosion) has been discussed by Rosner and Nagarajan (1987) and Miller et al. (1992).

A5. Roughness and target shape evolution. We have explicitly considered cases in which the "asymptotic" roughness associated with (quasi-) steady-state erosion is small, on the scale of the target radius of curvature, $d_t/2$, as must be the cumulative surface recession (cf. the numerical example in "'Direct' Use to Predict Erosion Behavior"). Indeed, this is fully compatible with the erosion yield data being used, which is itself averaged over long times (many impacts during the constant erosion rate period).

It is also possible to extract from the "lobular" polar plots of $E\{\theta, \ldots f'\}$ (Figure 5) what might be called the "shape evolution tendency." For the cases shown (when $f'\{0\} > 0$ and f_0 small compared to unity but positive; Figure 2) there is an initial tendency to reduce to zero the stagnation "line" radius of curvature and exhibit comparatively rapid surface recession in the vicinity of $\theta_{E_{max}} (> 0)$. *This corresponds to a tendency to make an initially circular-cylindrical metal leading "edge" (nose-region) "wedge"-shaped as time proceeds*—an outcome that has been reported frequently in the experimental erosion literature.

A6. "Log-normal" distribution of abrasive particles in the mainstream. For our theoretical formulation/numerical calculations and graphical output we have assumed that the mainstream abrasive particle size distribution, or at least that portion of it that corresponds to supercritical Stokes numbers in the prevailing environment, is "log-normal," that is, that the distribution function $vC\{v\}$ is Gaussian on semi-log (linear $vC\{v\}$ vs. $\log_{10} v$) paper, characterized by the two parameters σ_g (spread) and v_g. While it would be straightforward to carry out the required numerical quadratures with other single-mode size distributions (e.g., Rosin-Rammler; cf. Khail and Rosner, 1995), this particular two-parameter choice is sufficiently versatile and computationally convenient (cf. Rosner and Tassopoulos, 1989). Of particular theoretical significance is the fact that even initially "mono-dispersed" (Dirac *pdf*) populations will evolve by Brownian coagulation into near log-normal populations with, for example, $\sigma_g \approx 2.3$ (while we use the parameter σ_g to characterize the *spread* (variance) of the log-normal population, we have chosen to report our results in terms of the number-mean particle volume $\bar{v} (= \phi_p/N_p)$ rather than the value of which $vC\{v\}$ has its local maximum; these two volumes are related by Eq. 25 (see, e.g., Rosner and Tassopoulos, 1989) for the continuum (Smoluchowski) collision rate function (see, e.g., Friedlander, 1977). Moreover, if multimodal populations were relevant in an important class of erosion applications (see the next subsection), they could be represented by sums of single-mode contributions (e.g., log-normal or Rosin-Rammler).

Generalizations

It may be useful to itemize and comment upon particularly valuable *generalizations* of our present results, that is, ways to deal with somewhat more complex situations than those explicitly embraced in our physicomathematical model (see the subsection on basic assumptions). We hope these comments and conjectures can be exploited and tested soon, to further enlarge the domain of tractable engineering design problems in this general class, and thereby reduce the number of expensive "surprises" associated with erosion-induced failures.

Abrasive particle "blends". It is tempting to conjecture that if, as is common, the suspended particle population is actually a "blend" of several populations of rather different erosion propensity, the total erosion rate can be simply estimated as the sum of the contributions from each "subpopulation." We are unaware if this obvious approach has yet been put to the experimental test; however, the paper of Kotwal and Tabakoff (1981) is relevant here.

Interactions among "flanking" cylindrical targets. Recent studies (Konstandopoulos et al., 1993) have indicated that our "effective Stokes number" approach can be generalized to account for the first-order aerodynamic effects of adjacent target proximity. While this has been explicitly tested using predicted total particle *capture* rates for $s = 1$, it is reasonable to extend the notion to the estimation of target *erosion* rates. This approach is equivalent to imagining that each target is "isolated" but exposed to a fictitious dust-laden mainstream that gives rise to the same stagnation point inviscid velocity gradient as in the real tube bank.

Application to other important shapes/conditions. The observations of Israel and Rosner (1983) that inertial impaction behavior of qualitatively similar target shapes can be brought into near coincidence using an "effective Stokes number" based on the prevailing inverse inviscid stagnation point velocity gradient, suggests, for example, that our erosion rate prediction procedures developed and illustrated here for a *circular* cylinder might be used to estimate leading "edge" region erosion rates for turbine bladelike shapes (circular cylinder "forebody" with nearly flat "afterbody" (skirt)) by simply increasing all Stokes numbers (including the critical

Stokes number 1/8) by the approximate factor 1.08 to account for the effect of the afterbody in reducing the inviscid stagnation point velocity gradient in the absence of appreciable blade "camber" (backbone curvature) and associated fluid "circulation." In such applications it may also be necessary to correct for the systematic effects of nonnegligible *Mach number* of the approaching gas flow. Following Israel and Rosner (1983), this can be approximated by incorporating the effects of freestream Mach number on both the *flow time* and particle *stopping time* (by use of the gas viscosity evaluated in the stagnation region) in the calculation of the relevant particle Stokes number.

Quasi-steady application of "steady-state" results. In applications where the dust loading and gas stream conditions are *not* constant but changing sufficiently slowly on the time scale $(d_t/2)/U$, one can justifiably treat the total erosion (surface recession) as having been the result of target exposure in a "sequence" of "steady" environments and summing their effects.

Implicit effects (temperature, oxidizing/reducing environments, stress). The *framework* provided by the present analysis will clearly allow several "environmental" effects (e.g., effects of temperature level (e.g., Gat and Tabakoff, 1980)) to be (implicitly) included in the appropriate values of the three erosion yield parameters n, $f(0)$, and θ_* and $\epsilon_{p,\mathrm{ref}} \equiv \epsilon_p(V_{p,\mathrm{ref}}, \theta_*)$ ($V_{p,\mathrm{ref}} = 100$ m/s, say) for particular combinations of projectile/target materials (see e.g., Kho et al. (1994)) (irrespective of whether an adequate theory is yet available to anticipate or extrapolate such effects). Another potentially important variable (which has evidently not yet been considered in erosion yield measurements) is the *state of stress* in the target material surfaces. For example, one would expect preexisting tensile stresses to be particularly important in the case of somewhat brittle materials.

However, we can easily anticipate erosion/corrosion situations that may require fundamental generalizations of the present approach, that is, when the time scales of metal oxide layer (re-)growth and successive projectile impacts are comparable. Such situations would probably give rise to a particle flux dependence of the average erosion yield, not contained in the present formulation.

Particle size dependence of erosion yield? Several sets of erosion yield data in the literature (e.g., Figure 5 of Kotwal and Tabakoff, 1981) reveal a nonnegligible particle size dependence, especially for "small" projectiles (e.g., below about 30 μm in Kotwal and Tabakoff, 1981). This would cause the procedures of the subsection on erosion rates to systematically overestimate erosion rates. However, inspection of Eq. 8 reveals that, if one were convinced that such an effect were not merely an artifact of the particular erosion yield experiment itself, it could be easily incorporated in the indicated quadrature expression via a suitably generalized ϵ_p-expression.

Velocity exponent sensitivity to angle-of-incidence. The "separability" of V_p and θ_i-effects in the erosion yield law $\epsilon_p(V_p, \theta_i)$ significantly reduces the number of dimensionless parameters appearing in our final results and, hence, increases the attractiveness of our "short-cut" procedure. However, there appear to be systems (combination of projectile/target materials) for which the velocity exponent n increases noticeably with angle-of-incidence (see, e.g., Tabakoff et al., 1988). For such systems the "shape" function $f(\theta_i)$ would not quite be the same at all impact velocities, another complexity that could be straightforwardly introduced, if indeed necessary, into our quadrature procedure.

Threshold velocity for erosion damage. It is generally not possible to formally extrapolate the power-law velocity dependence of ϵ_p very far *below* the range of actual erosion rate measurements because of the likely existence of a *threshold velocity* below which no perceptible erosion (substrate loss) occurs. In effect, our previous procedures ("Erosion Yield Law") are based on the sequence of inequalities:

$$\text{Sound speed in target} \gg V_p(\le O(U))$$

$$\gg V_p(\text{erosion threshold}) \gg V_p(\text{critical (for capture)})$$

and will inevitably overestimate erosion rates when these rates are very small (e.g., near $Stk_{\mathrm{crit,eff}} \approx 1/8$). Again, this systematic effect could be incorporated if a more general $\epsilon_p(V_p, \theta_i)$ law were used in our quadratures.

Conclusions, Future Work

By combining the essential features of available erosion yield experiments (where small flat specimens are successively exposed to size-selected particles impacting at particular velocities and incidence angles) with what is now known about the inertial impaction of particles on a circular cylinder in high Reynolds number cross-flow, we have developed and illustrated here an efficient approximate method to predict total surface erosion rates for such targets exposed to a distribution of abrasive particles suspended in the mainstream. While "universal" graphs are provided to cover the anticipated dimensionless parameter ranges of greatest current interest, the required correlation formulas and quadrature expressions are also provided to be able to deal with any "singular" cases of particular interest to the reader. We have also indicated a number of feasible generalizations that seem likely to be of interest in future applications.

Among other things, our results make it clear that while erosion rates will usually be directly proportional to the abrasive particle number density in the mainstream, erosion rates will be more sensitive to mainstream velocity than the usually assumed U^{n+1} dependence (where, often, $n \approx 2.5$). They also explain why initially blunt metal bodies become "sharpened," or even wedge-shaped, as a result of erosion, and when enlarged nose radii will be an effective "ruggedization" strategy.

The erosion rate prediction procedures suggested and illustrated here are probably efficient enough to be incorporated into future improved "*erosion propensity*" *indices*. Even indices that are manifestly less complete have been used to help quantify the costs and benefits of using coals of various quality in power stations and furnaces (see, e.g., Raask, 1985).

Our approach and some of our results may also be useful in extrapolating the performance of machining/cutting devices based on the use of high-speed jets of liquid slurries or gas-suspensions of abrasive powder. An effective Stokes number based on the reciprocal of the stagnation point velocity gradient (see Israel and Rosner, 1983) would again provide the link to our present analysis (see the subsection titled "Generalizations"). A useful extension would be an erosion

rate theory applicable to the duct walls of pneumatic transport systems (Arundel et al., 1973), including high volume fraction turbulent slurries.

Also of future interest, and perhaps closer to the present article, would be the development of a comparable rational theory to predict erosion rates for targets immersed in (rather than downstream of) bubbling *fluidized beds* (Tossaint et al., 1990; Zhu et al., 1991)—a daunting problem due to the apparent failure of many assumptions (see the subsection on basic assumptions) underlying the present analysis (e.g., A1, A4). Still closer to our present analysis and currently under investigation is the situation encountered in the refractory interior walls of high temperature cyclones in circulating fluidized bed combustion systems (Elliot, 1994; Khail and Rosner, 1995).

In closing, we mention another extension of this approach; that is, the deliberate "scouring" of thin but adherent granular deposits on heat exchanger—or turbine blade—surfaces. When it becomes possible to specify the appropriate erosion yield behavior for such a "solid" exposed to the scouring projectiles of choice (usually those that will leave the underlying metal undamaged), then the time required to "remove" such deposits (to an acceptable degree) could be anticipated using an obvious variant of the present formulation. This information may become available via extensions of our numerical treatment of the "micromechanics" of particle interactions (capture, erosion) with granular deposits (see, e.g., Rosner et al., 1992; Konstandopoulos, 1991; Rosner and Nagarajan, 1987). Results of this type would also make possible the rational prediction of self-regulating quasi-steady-state deposit thicknesses of ash-laden situations in which there is broad (or bimodal) size distribution, with *simultaneous deposition and deposit erosion* (see, e.g., Rosner and Nagarajan, 1987; Rosner et al., 1983; Wagoner and Yan, 1992; and Miller et al., 1992).

Acknowledgments

This research was supported in part by DOE-PETC (Grant DE-FG-2290PC90099, concluded Oct. 31, 1994) and AFOSR (Grant 91-0170), as well as the Yale HTCRE Laboratory Industrial Affiliate, Dupont. It is also a pleasure to acknowledge helpful discussions and/or correspondence with J. Fernandez de la Mora, Y. F. Khalil, and A. G. Konstandopoulos.

Notation

c = constant in Eq. 15 (= 0.158)
d_p = particle diameter, $(6v/\pi)^{1/3}$
f = normalized angle of incidence dependence of erosion yield function, Eq. 2
f_0 = normalized erosion yield at normal incidence; Figure 3 ($\equiv f(0)$)
k = "order" of PSD moment
Kn = Knudsen number (ratio of *particle* mean-free-path to d_t)
n = erosion yield velocity exponent
n_{eff} = $(\partial \ln ER/\partial \ln U) - 1$
$n(v)$ = particle number density distribution function, dN_p/dv
q = order of partial moment of log-normal distribution, Eq. 37
s = capture fraction upon local impaction
$\bar{U}$ = time-averaged mainstream velocity when U is "fluctuating"
v_g = median volume of log-normal distribution of particles

Greek letters

α = lower limit of partial moment of log-normal distribution
β = upper limit of partial moment of log-normal distribution
μ = dynamic viscosity of carrier gas
ν = gas momentum diffusivity (μ/ρ_g)
θ_i = local impingement angle with respect to local normal (cf. Figure 1)
ρ_g = gas density
ρ_p = density of each particle
$\{\ \}$ = argument of function

Literature Cited

Arundel, P. A., I. A. Taylor, and W. Dean, "The Rapid Erosion of Various Pipe Wall Materials by a Stream of Abrasive Alumina Particles," *Pneumotransport*, **2**, Paper E1 1–15 (1973).

Beacher, B., W. Tabakoff, and A. Hamed, "Improved Particle Trajectory Calculations Through Turbomachinery Affected by Coal Ash Particles," *ASME, 81-GT-53* (1981).

Bitter, J. G. A., "A Study of Erosion Phenomena," *Wear*, **13** (1963).

Brun, R. J., W. Lewis, P. J. Perkins, and J. S. Serafini, *NACA Rep. 1215* (1955).

Brun, R. J., J. S. Serafini, and H. M. Gallagher, *NACA Tech. Note 2903* (1953).

Engel, P. A., "Impact Wear of Materials," *Tribology Ser. 2*, Elsevier, Amsterdam (1978).

Elliot, T., "Shoot for More Durable, Less Costly Refractory in CFB Units," *Power*, 69 (1994).

Fernandez de la Mora, J., and D. E. Rosner, "Effects of Inertia on the Diffusional Deposition of Small Particles to Spheres and Cylinders at Low Reynolds Numbers," *J. Fluid Mech.*, **125**, 379 (1982).

Fernandez de la Mora, J., and D. E. Rosner, "Inertial Deposition of Particles Revisited and Extended: Eulerian Approach to a Traditionally Lagrangian Problem," *J. PhysicoChemicalHydrodynam.*, **2**, 1 (1981).

Finnie, I., "An Experimental Study of Erosion," *Proc. Soc. Experimental Stress Analysis*, **17**(2), 65–70 (1959); see also ASTM Spec. Tech. Public #307, 70 (1962); *Wear*, **3**, 87 (1960); *J. Mat.*, **2**(3), 682 (1967).

Friedlander, S. K., *Smoke, Dust and Haze—Fundamentals of Aerosol Behavior*, Wiley, New York (1977).

Fuchs, N. A., *The Mechanics of Aerosols*, Pergamon, New York (1964).

Gat, N., and W. Tabakoff, "Effect of Temperature on the Behavior of Metals Under Erosion by Particulate Matter," *J. Test Eval.*, **8**, 177 (1980).

Israel, R., and D. E. Rosner, "Use of Generalized Stokes Number to Determine the Aerodynamic Capture Efficiency of Non-Stokesian Particles from a Compressible Gas Flow," *Aerosol. Sci. Tech.*, **2**, 45 (1983).

Khalil, Y. F., and D. E. Rosner, "Erosion Rate Prediction Technique for Ceramic Surfaces Exposed to High Speed Flows of Abrasive Suspensions," *J. Amer. Ceramic Soc.*, submitted (1995).

Kho, T., D. E. Rosner, and P. Tandon, "Simplified Erosion Rate Prediction Technique for Cylindrical Metal Targets in the Cross-Flow of Abrasive Suspensions," ASME *J. Propul. Power*, submitted (Summer, 1994).

Konstandopoulos, A. G., M. Labowsky, and D. E. Rosner, "Inertial Deposition of Particles from Potential Flows Past Cylinder Arrays," *J. Aerosol Sci.*, **24**(4), 471 (1993).

Konstandopoulos, A. G., and D. E. Rosner, "Inertial Effects on Thermophoretic Transport of Small Particles to Walls with Streamwise Curvature: I. Experiments; II. Theory," *Int. J. Heat Mass Trans.*, in press (1995).

Kotwal, R., and W. Tabakoff, "A New Approach for Erosion Prediction Due to Fly Ash," *J. Eng. Power*, **103**, 263 (1981).

Menguturk, M., and E. F. Sverdrup, "Calculated Tolerance of a Large Electric Utility Turbine to Erosion Damage by Coal Gas Ash Particles," *Westinghouse R & D Center, 77-1E3-CEDRM-P2* (1977).

Menguturk, M., and D. Günes, "Blade Boundary Layer Effects on Turbine Erosion and Deposition," *ASME Trans.—J. Fluid Eng.*, **106**, 113 (1984).

Menguturk, M., and E. F. Sverdrup, "Calculated Tolerance of a Large Electric Utility Turbine to Erosion Damage by Coal Gas Ash Particles," *Proc. ASTM Symposium on Erosion: Prevention and Useful Applications*, 1 (1977).

Miller, E., A. L. Yarin, and Y. Goldman, "Competition between

Thermophoretic Deposition and Erosion, Leading to Appearance of Steady Coating," *J. Aerosol Sci.*, **23**(2), 97 (1992).
Park, H. M., and D. E. Rosner, "Combined Inertial and Thermophoretic Effects on Particle Deposition Rates in Highly Loaded Dusty Gas Systems," *Chem. Eng. Sci.*, **44**(10), 2233 (1989).
Raask, E., *Mineral Impurities in Coal Combustion*, Hemisphere, Washington, DC (1985).
Raask, E., "Tube Erosion by Ash Impaction," *Wear*, **13**, 301 (1969).
Rosner, D. E., and J. Fernandez de la Mora, "Correlation and Prediction of Thermophoretic and Inertial Effects of Particulate Deposition from Non-Isothermal Turbulent Boundary Layers," in *Particulate Laden Flows in Turbomachinery*, W. Tabakoff, C. T. Crowe, and D. B. Cale, eds., ASME, 85 (1982).
Rosner, D. E., and J. Fernandez de la Mora, "Boundary Layer Effects on Particle Impaction and Capture," *ASME Trans., J. Fluid Eng.*, **106**, 113 (1984).
Rosner, D. E., D. Günes, and N. Nazih-Anous, "Aerodynamically-Driven Condensate Layer Thickness Distributions on Isothermal Cylindrical Surfaces," *Chem. Eng. Commun.*, **24**, 275 (1983a).
Rosner, D. E., S. Gökoglu, and R. Israel, "Rational Engineering Correlations of Diffusional and Inertial Particle Deposition Behavior in Non-Isothermal Forced Convection Environments," in *Fouling and Heat Exchanger Surfaces*, R. Bryers, ed., Eng. Foundation, New York, 235 (1983).
Rosner, D. E., *Transport Processes in Chemically Reacting Flow Systems*, Butterworth-Heinemann, 3rd printing, Stoneham, MA (1990).
Rosner, D. E., and R. Nagarajan, "Toward a Mechanistic Theory of Net Deposit Growth from Ash-Laden Flowing Combustion Gases: Self-Regulating Sticking of Impacting Particles and Deposit Erosion in the Presence of Vapor Glue," *Proc. Heat Transfer Conf.*, R. W. Lyczkowski, ed., *AIChE Symp. Ser.*, **83** (257), 289 (1987).
Rosner, D. E., "Total Mass Deposition Rates from 'Polydispersed' Aerosols," *AIChE J.*, **35**(1), 164 (1989).
Rosner, D. E., and M. Tassopoulos, "Deposition Rates from 'Polydispersed' Particle Populations of Arbitrary Spread," *AIChE J.*, **35**(9), 1497 (1989).
Rosner, D. E., A. G. Konstandopoulos, M. Tassopoulos, and D. W. Mackowski, "Deposition Dynamics of Combustion Generated Particles: Summary of Recent Studies of Particle Transport Mechanisms, Capture Rates and Resulting Deposit Microstructure Properties," *Proc. Engineering Foundation Conf.: Inorganic Transformations and Ash Deposition During Combustion*, ASME/Engineering Foundation, 585 (1992).
Rosner, D. E., P. Tandon, and A. G. Konstandopoulos, "Rapid Estimation of Deposition Rates on Cylinders in Dust-Laden Streams: Effect of Single Particle Capture Law and Dust Polydispersity on Predicted Local and Total Deposition Rates," Yale HTCRE Lab. Publication #202, *Chem. Eng. Sci.*, in press (1995).
Rosner, D. E., and P. Tandon, "Effective Stokes Number Correlation of Particle Cyclone Separator Performance and an Improved Method to Estimate the Capture Efficiency Characteristics of Large, Geometrically Similar Cyclones Operating Away From Calibration Conditions," Yale HTCRE Lab. Publication #200, in preparation (Summer, 1994).
Rosner, D. E., P. T. Tandon, and A. G. Konstandopoulos, "Local Size Distributions of Particles Deposited by Inertial Impaction From Polydispersed Particle-Laden Streams," *J. Aerosol Sci.*, in press (1995).
Tabakoff, W., J. Ramachandran, and A. Hamed, "Temperature Effects on the Erosion of Metals Used in Turbomachinery," *Proc. 5th Int. Conf. on Erosion by Solid and Liquid Impact*, 47-1 (1979a).
Tabakoff, W., R. Kotwal, and A. Hamed, "Erosion Study of Different Materials Affected by Coal Ash Particles," *Wear*, **52**, 161 (1979b).
Tabakoff, W., J. Ramachandran, and A. Hamed, "Study of Metal Erosion in High Temperature Coal Gas Streams," *Eng. Power*, **102**(1), 148 (1980).
Tossaint, H. H. J., and P. P. van Norden, "Fluidized Bed Tube Bank Erosion and Flow Visualization," *Multiple Transport and Particle Phenomena*, T. N. Veziroglu, ed., Vol. 3, Hemisphere, 365 (1990).
Wagoner, C. L., and X. X. Yan, "Deposit Initiation via Thermophoresis: 1. Insight on Deceleration and Retention of Inertially Transported Particles," *Proc. Engineering Foundation Conf.: Inorganic Transformation and Ash Deposition During Combustion*, ASME/Engineering Foundation, 607 (1992).
Wang, H. C., "Theoretical Adhesion Efficiency for Particles Impacting a Cylinder at High Reynolds Number," *J. Aerosol. Sci.*, **17**(5), 827 (1986).
Wessel, R. A., and J. Righi, "Generalized Correlations for Inertial Impaction of Particles on a Circular Cylinder," *Aerosol Sci. Tech.*, **9**, 26 (1988).
Zhu, J., C. J. Lim, J. R. Grace, and J. A. Lund, "Tube Wear in Gas Fluidized Beds: II. Low Velocity Impact Erosion and Semi-Empirical Model for Bubbling and Slugging Fluidized Beds," *Chem. Eng. Sci.*, **46**(4), 1151 (1991).

Manuscript received Jan. 31, 1994, and revision received June 10, 1994.